PHYSICAL REVIEW C VOLUME 9, NUMBER 6 JUNE 1974

Effect of deuteron breakup on elastic deuteron-nucleus scattering

George H. Rawitscher*
Center for Theoretical Physics, Massachusetts Institute of Technology, Cambridge, Massachusetts 02139,† and Department of Physics, University of Surrey, Guildford, Surrey, England

(Received 1 October 1973; revised manuscript received 4 March 1974)

The properties of the transition matrix elements $V_{ab}(R)$ of the breakup potential V_N taken between states $\phi_a(\vec{r})$ and $\phi_b(r)$ are examined. Here $\phi_a(\vec{r})$ are eigenstates of the neutron-proton relative-motion Hamiltonian, and the eigenvalues of the energy ϵ_a are positive (continuum states) or negative (bound deuteron); $V_N(\vec{r}, \vec{R})$ is the sum of the phenomenological proton nucleus $V_{p-A}(|\vec{R}-\frac{1}{2}\vec{r}|)$ and neutron nucleus $V_{n-A}(|\vec{R}+\frac{1}{2}\vec{r}|)$ optical potentials evaluated for nucleon energies equal to half the incident deuteron energy. The bound-to-continuum transition matrix element for relative neutron-proton angular momenta $l=2$ are found to be comparable in magnitude to the ones for $l=0$ for values of ϵ_a larger than about 3 MeV, and both decrease only slowly with ϵ_a, suggesting that a large breakup spectrum is involved in deuteron-nucleus collisions. The effect of the various breakup transitions on the elastic phase shifts is estimated by numerically solving a set of coupled equations. These equations couple the functions $\chi_a(\vec{R})$ which are the coefficients of the expansion of the neutron-proton-nucleus wave function in a set of the $\phi_a(\vec{r})$'s. The equations are rendered manageable by performing a (rather crude) discretization in the neutron-proton relative-momentum variable k_a. Numerical results for 21.6-MeV deuterons incident on Ni and Ca which include only the first momentum bin ($\epsilon_a \leq 10$ MeV) and $l=0$ and 2 show that the effects on the elastic phase shifts are similar in several respects to those found by Johnson and Soper.

[NUCLEAR REACTIONS Elastic deuteron-nucleus scattering theory. Effect of deuteron breakup. Numerical applications to $E=21.6$ MeV d-Ca and d-Ni.]

I. INTRODUCTION

Several attempts have recently been made to include the effect of breakup on the elastic scattering of deuterons from nuclei. Among them are several which do not attempt to include the full three-body treatment, but rather try to stay closer to the two-body optical model formalism.[1-4] The present study falls into the same category. Particularly the work of Johnson and Soper,[3] to be referred to as JS in what follows, has raised a good deal of interest because of its success in improving the distorted-wave Born-approximation (DWBA) predictions for stripping and pickup reactions.[5] The idea of JS is to consider a wave function $\bar{\chi}(\vec{R})$ which describes the motion of the center of mass of the neutron-proton pair relative to the nucleus. This wave function contains simultaneously the bound-deuteron (elastic) component as well as some portion of the breakup components. The assumption which makes it possible to include both bound and breakup components simultaneously into one function $\bar{\chi}(\vec{R})$ is that, for low energies ϵ_k of relative neutron-proton motion, the relative n-p wave function $\phi_k(\vec{r})$ is quite similar to the bound-deuteron wave function $\phi_b(r)$ for small values of the n-p distance $\vec{r}$. Here

$$\vec{R}=\tfrac{1}{2}(\vec{r}_n+\vec{r}_p), \quad \vec{r}=\vec{r}_n-\vec{r}_p, \tag{1}$$

and $\vec{r}_n$ and $\vec{r}_p$ are the position vectors of the neutron and proton, respectively, relative to the center of the target nucleus. By replacing the energies ϵ_k by the bound-state energy ϵ_b, JS manage to obtain a single local Schrödinger equation for $\bar{\chi}(\vec{R})$. For the calculation of the DWBA stripping matrix element, knowledge of the neutron-proton wave function for only small distances of r is required because of the appearance of the short-ranged neutron-proton potential $V_{np}(r)$ in the integrand, and hence the use of $\bar{\chi}(\vec{R})$ in the stripping matrix element has a good deal of validity. For the calculation of the deuteron elastic scattering phase shifts however, the bound-deuteron component has to be extracted from $\bar{\chi}$, which JS accomplish by solving a set of two coupled equations. For the calculation of elastic scattering the assumption that only the low-energy breakup spectrum enters significantly into the full n-p wave function is more questionable than for the stripping calculation, because larger values of r are involved in the former. Nevertheless, even for the stripping calculation it is of interest to investigate the extent of the neutron-proton relative momentum breakup spectrum which is excited when a deuteron impinges upon a nucleus.

It is the purpose of this investigation to examine the above question by calculating the breakup ma-

trix elements for transitions between the bound to the breakup neutron-proton states, both as a function of the relative neutron-proton momenta k, as well as for several values of the relative neutron-proton angular momenta l.[6] These matrix elements are calculated numerically for 21.6-MeV deuterons incident on the nuclei of nickel and calcium, and are also calculated analytically under simplified conditions in order to obtain a better idea of their k and l dependence. These matrix elements are functions of R and play the role of coupling potentials in the set of coupled equations for the functions $\chi_k(\vec{R})$ which describe the motion of the broken-up neutron-proton pair relative to the nucleus. These coupled equations are very difficult to handle since the functions $\chi_k(\vec{R})$ depend on the continuous index k, and also because some of the coupling potentials are of quite long range in R. Nevertheless, in order to obtain an idea of how strongly the breakup spectrum affects the elastic scattering phase shifts, the coupled equations are subjected to a crude discretization in k space, the momentum expansion is truncated at $k \geq k_{\max}$, and the resulting coupled equations are solved numerically. Although the expansion in momentum space is expected to converge satisfactorily (as $k_{\max}^{-3}$ or $k_{\max}^{-4}$), the choice of $k_{\max} = 0.5$ fm^{-1} was still found not to be large enough in the present example; for this and various additional reasons the numerical illustration still lacks realism. However, it should be kept in mind throughout that the purpose of the present calculation is to cast some light on the nature and the extent of the breakup spectrum excited during deuteron-nucleus collisions. The hope is to thereby clarify the nature of the approximations suitable in the evaluation of rigorous theories of either the elastic scattering, the stripping, or the breakup reaction.

II. THE FORMALISM

A. General discussion

The wave function describing the neutron and proton in the presence of the target nucleus is denoted by $\Psi(\vec{r}, \vec{R})$. The internal coordinates of the nucleons in the target nucleus are not explicitly indicated. The antisymmetrization of the wave function for interchange of the incident nucleons with the nucleons in the target is ignored. The effect of antisymmetrization has been investigated by several authors,[7,8] and for deuterons with incident energy larger than about 15 MeV the effect was found to be small.

A complete set of eigenstates $\phi_k^{(l,m)}(\vec{r})$ of the neutron-proton Hamiltonian (in the absence of the nucleus) $H_{np}(r)$,

$$H_{np}(r) = T_r + V_{np}(r), \tag{2}$$

$$(H_{np} - \epsilon_k)\phi_k^{(l,m)}(\vec{r}) = 0, \tag{3}$$

is now introduced. Here T_r is the kinetic-energy operator of relative neutron-proton motion, V_{np} is a neutron-proton potential, k and l are the neutron-proton relative linear and angular momenta, respectively, and m is the projection of l along the z axis. All nucleon spins are disregarded, and the potential $V_{np}(r)$ is taken to refer to the triplet isospin zero nucleon-nucleon state, represented by a local Gaussian potential[9]

$$V_{np}(r) = -V_0 \exp(-\alpha r^2), \quad V_0 = 66.92 \text{ MeV}, \quad \alpha = 0.415 \text{ fm}^{-2}, \tag{4}$$

which adequately represents the low-energy nucleon-nucleon properties. In the absence of tensor forces the radial components $u_l(k,r)$ of $\phi_k^{(lm)}$

$$\phi_k^{(l,m)}(\vec{r}) = r^{-1}u_l(k,r)Y_{lm}(\hat{r}) \tag{5}$$

obey simple uncoupled radial Schrödinger equations and are assumed to have the asymptotic form

$$u_l(k,r) \sim (2/\pi)^{1/2} \sin(kr - \tfrac{1}{2}l\pi + \delta_l), \tag{6}$$

where the δ_l's are the elastic real scattering phase shifts. The above normalization insures that

$$\int \phi_k^{(l,m)}\phi_{k'}^{(l',m')}d^3r = \delta_{mm'}\delta_{ll'}\delta(k-k'). \tag{7}$$

The bound-state solution of Eq. (3) is denoted by the subscript b, $\phi_b(\vec{r}) = r^{-1}u_b(r)Y_{00}(\hat{r})$. It is normalized to unity (i.e., $\int_0^\infty |u_b|^2 dr = 1$) and is orthogonal to all ϕ_k's. The energies ϵ_b and ϵ_k have the value -2.225 MeV and k^2/m for the bound and continuum cases, respectively. The expansion of the wave function $\Psi(\vec{r}, \vec{R})$ in terms of the ϕ_k's is as follows:

$$\Psi(\vec{R}, \vec{r}) = \chi_b(\vec{R})\phi_b(r) + \sum_{l,m} \int dk\, \chi_k^{(l,m)}(\vec{R})\phi_k^{(l,m)}(\vec{r}). \tag{8}$$

An expansion of this type is very old.[10] The coefficients χ_k of the above expansion are functions of $\vec{R}$ to be determined from the solution of a set of coupled equations which follow from the Schrödinger equation, as is discussed below. The boundary conditions for the χ's, for the case of incident deuterons are that, asymptotically, χ_b has both incident and outgoing waves and the χ's only outgoing waves.

The Schrödinger equation is

$$[T_R + V_N(\vec{R}, \vec{r}) + H_{np} - E]\Psi(\vec{r}, \vec{R}) = 0, \tag{9}$$

where the potential V_N is given by the sum of the

nucleon-nucleus optical potentials

$$V_N(\vec{R},\vec{r}) = V_{p-A}(|\vec{R}-\tfrac{1}{2}\vec{r}|) + V_{n-A}(|\vec{R}+\tfrac{1}{2}\vec{r}|) \qquad (10)$$

and T_R is the kinetic-energy operator in the variable $\vec{R}$. The internal degrees of freedom of the nucleus are embodied in the potentials V_{p-A} and V_{n-A}, which are chosen to be the complex phenomenological nucleon-nucleus optical potentials at a nucleon incident energy equal to half the deuteron energy. For the incident bound deuteron the correction to Eq. (10) due to the internal motion of the nucleons in the deuteron is estimated[11] to be less than 10%. However, for the high relative n-p momenta this choice of the V's in Eq. (10) is increasingly suspect.[12] In particular, for negative nucleon-nucleus relative energies V_{n-A} should become real and admit bound states—a possibility not allowed by the choice of the V's in Eq. (10).

Equation (9) can be rewritten in the Lippmann-Schwinger form

$$\Psi(\vec{r},\vec{R}) = e^{i\vec{k}_0\cdot\vec{R}}\phi_b(r) + \int d^3r'\, d^3R'\, G_E^{(+)}(\vec{R},\vec{r};\vec{R}'\vec{r}')\, V_N(\vec{R}'\vec{r}')\Psi(\vec{r}',\vec{R}'), \qquad (11)$$

where $G_E^{(+)}$ is the three-body Green's function

$$G_E^{(+)}(\vec{R},\vec{r};\vec{R}'\vec{r}') = \sum_{l,m}{}' \int dk\, \phi_k^{(l,m)}(\vec{r})\phi_k^{(l,m)*}(\vec{r}') \times g_0^{(+)}(E-\epsilon_k,\vec{R},\vec{R}'). \qquad (12)$$

Here $g_0^{(+)}$ is the free two-body Green's function with outgoing wave boundary conditions, the functions ϕ_k were defined in Eqs. (3), (5), and (6), the symbol $\int'$ in Eq. (12) indicates that the bound state ϕ_b is to be included in the expansion, and $\vec{k}_0$ in Eq. (12) represents the incident-deuteron momentum.

The representation of $G_E^{(+)}$ given by Eq. (12) has been given, for example, by Newton,[13] Glöckle,[13] and Takeuchi.[14] This representation for $G_E^{(+)}$ is equivalent to the expansion of $\Psi(\vec{R},\vec{r})$ given by Eq. (8), together with the outgoing wave boundary condition for the χ_k's. The use of $G_E^{(+)}$ given by Eq. (12) assures that the correct outgoing boundary conditions in the breakup channel are satisfied; however, no assurance can be given that the proper boundary conditions in the stripping channels are obtained. For this purpose additional equations with different Green's functions are required.[13,14] If, as will be done later on, the expansion given by Eq. (8) is truncated by admitting only a finite number of partial waves in the relative angular momenta of the coordinates $\vec{r}$ and $\vec{R}$, $l \le l_{\max}$, and $L \le L_{\max}$, respectively, and breaking off the integration over k at a finite upper limit $k_{\max}$, then the resulting truncated wave function $\Psi^T(\vec{r},\vec{R})$ contains no stripping components in the asymptotic region. This can be seen by noting that the asymptotic behavior of Ψ^T for large r and R (apart from the plane-wave component of χ_b) is of the form $r^{-1}R^{-1}$, which when translated to the coordinates r_n and r_p gives rise to $(r_p)^{-2}$ for r_n finite, in contradiction with the expected asymptotic $(r_p)^{-1}$ behavior of a (d,p) stripping channel. The function $\Psi^T(r,R)$ thus does not describe the full three-body properties of the n-p nucleus system.

B. The coupled equations

By introducing the bipolar harmonics[15]

$$Y_{(lL)JM_J}(\hat{r},\hat{R}) = \sum_{m,M}\langle JM_J \mid lLmM\rangle Y_{LM}(\hat{R})Y_{lm}(\hat{r}), \qquad (13)$$

where $\langle a\alpha/bc\beta\gamma\rangle$ are Clebsch-Gordan coefficients, and introducing the radial functions $f_{(lL)JM_J}(k,R)$ as the coefficients in a spherical harmonic expansion of $\chi_k^{(l,m)}(\vec{R})$, then the truncated form, Eq. (8), of the expansions of Ψ can be rewritten as

$$\Psi^T(\vec{R},\vec{r}) = \frac{1}{Rr}\sum_{lLJM_J}^{l_{\max},L_{\max}} \int_0^{'K_{\max}} dk\, u_l(k,r) f_{(lL)JM_J}(k,R) Y_{(lL)JM_J}, \qquad (14)$$

where again the symbol $\int'$ means that the bound state $u_b(r)$ is also included.

By inserting Ψ^T given by Eq. (14) into Eq. (9), multiplying on both sides by $r^{-1}u_{l'}(k',r)Y_{(l'L')J'M'}$, and integrating over $d^3r\,d\Omega_R$, one obtains the coupled equations for the f's

$$[(T_R)_{L'} - (E-\epsilon_{k'})]f_{(l'L')JM_J}(k',R) + \sum_{\lambda lL}^{l_{\max},L_{\max}} C^{J\lambda}_{l'L';lL}\int_0^{'k_{\max}} V^{\lambda}_{l'l}(k',k,R) f_{(lL)JM_J}(k,R)dk = 0. \qquad (15)$$

Here $(T_R)_{L'}$ stands for $-(\hbar^2/4m)[d^2/dR^2 - L'(L'+1)/R^2]$, and the coefficients C are given by

$$C^{J\lambda}_{L'l';Ll} = (-)^{\lambda+J}[(2l'+1)(2l+1)(2L'+1)(2L+1)(2\lambda+1)]^{1/2}\begin{pmatrix} l' & \lambda & l \\ 0 & 0 & 0 \end{pmatrix}\begin{pmatrix} L' & \lambda & L \\ 0 & 0 & 0 \end{pmatrix}\begin{Bmatrix} l' & l & \lambda \\ L & L' & J \end{Bmatrix}. \tag{16}$$

The expressions in round or curly brackets in Eq. (16) are Wigner coefficients or six-j symbols, respectively.[15] The breakup matrix element $V^{\lambda}_{l'l}$ is defined by

$$V^{\lambda}_{l'l}(k',k,R) = \int_0^\infty u_{l'}(k',r)v_\lambda(R,r)u_l(k,r)dr\,, \tag{17a}$$

$$V^{l}_{0l}(b,k,R) = \int_0^\infty u_b(r)v_l(R,r)u_l(k,r)dr\,, \tag{17b}$$

where v_λ is the spherical-harmonic-expansion coefficient of V_N,

$$V_N(\vec{R},\vec{r}) = \sum_{\lambda,m}(4\pi)(2\lambda+1)^{-1/2}v_\lambda(R,r)Y^*_{\lambda m}(\hat{R})Y_{\lambda m}(\hat{r})\,. \tag{18}$$

The functions $V^{\lambda}_{l'l}$ are the main objects of the present investigation. The coefficients C are the same "geometric" factors as the ones which occur in inelastic α-nucleus coupled-channel calculations. For example, for the case of the collective rotational or vibrational model the functions $V^{\lambda}_{l'l}(R)$ are replaced by the inelastic transition matrix elements

$$V^{\lambda}_{l'l}(R) \to \left(\frac{\beta_\lambda}{\sqrt{4\pi}}\right)\frac{R\partial V_{\mathrm{OM}}(R,R_{\mathrm{OM}})}{\partial R_{\mathrm{OM}}} \tag{19}$$

(to lowest order in the deformation parameter β_λ), R_{OM} being the radial fall-off parameter of the α-nucleus optical potential V_{OM}, and λ giving the multipolarity of the deformation β_λ of the nuclear optical potential. The coefficients C have the property

$$\sum_L (C^{Jl}_{J0;\,lL})^2 = 1\,.$$

III. BREAKUP POTENTIALS

A. General properties

The bound-to-continuum and the continuum-to-continuum breakup potentials are defined in Eqs. (17). They are denoted by $V^{\lambda}_{ll'}(k,k',R)$ and $V^{l}_{0l}(b,k,R)$, respectively, and serve as the potentials which couple the various radial functions $f_{(lL)JM_J}(k,R)$ in Eqs. (15). They are also called "transition matrix elements" in what follows. The k and l dependence of these potentials determines the feasibility of solving the coupled equations, Eqs. (15). For example, if $V^{l}_{0l}(b,k,R)$ decreases rapidly with increasing k and l, then only a small range of the breakup continuum is expected to affect the bound (deuteron) distorted-wave behavior. It is the purpose of this section to discuss some of the properties of the breakup potentials. Unless explicitly stated otherwise, only the contribution to the breakup potentials from the nuclear part of $V_N(\vec{R},\vec{r})$ will be considered.

One of the notable properties of the continuum-to-continuum transition potential is that for large values of R it decreases with R only very slowly (like R^{-2} under certain conditions), while the bound-to-continuum potential decreases much faster. This property can be understood by first considering the behavior of $v_\lambda(R,r)$, defined in Eq. (18), and then considering the integral in Eq. (17) defining $V^{\lambda}_{ll'}(R)$. For the purposes of this discussion $V_N(\vec{R},\vec{r})$, defined in Eq. (10), will be replaced by $V_{p-A}(|\vec{R}-\frac{1}{2}\vec{r}|)$, and the function V_{p-A} will be assumed to be of short range, i.e., V_{p-A} will be assumed negligible when $r_p(\vec{r}_p = \vec{R} - \frac{1}{2}\vec{r})$ is larger than the nuclear radius a. Under these conditions it will now be shown that when $R \gg a$, $v_\lambda(R,r)$ is negligible when r lies outside the interval $R-a<r<R+a$, and, further, when r lies in that interval the value of $v_\lambda(R,r)$ has the order of magnitude $(a/R)^2$. This can be seen by noting that Eq. (18) implies that

$$v_\lambda = \tfrac{1}{2}(2\lambda+1)^{1/2}\int_{-1}^{+1} V_N(\vec{R},\vec{r})P_\lambda(x)dx \tag{20}$$

where $x = \hat{r}\cdot\hat{R} = (r_p^2 - R^2 - \frac{1}{4}r^2)/Rr$ is the cosine of the angle θ_{rR} between $\vec{r}$ and $\vec{R}$. When $R \gg a$ and when V_N is replaced by $V_{p-A}(r_p)$, the integrand in Eq. (20) is large only when $r_p < a$, i.e., when both $R-a<\frac{1}{2}r<R+a$ and x is very close to unity, i.e., $1 \geq x > 1 - a^2/Rr$. The main contribution to the integral in Eq. (20) thus comes from a small region of size a^2/Rr near the upper limit, and thus the value of the integral itself is of the order of $V_{p-A}a^2/Rr$. This result can be made more rigorous by changing the variable x to r_p in Eq. (20). By using $dx = -2r_p dr_p/(Rr)$, one obtains the result

$$v_\lambda(R,r) = (2\lambda+1)^{1/2}(Rr)^{-1}\int_{|R-\frac{1}{2}r|}^{R+\frac{1}{2}r} V_{p-A}(r_p)P_\lambda(x)r_p dr_p\,. \tag{21}$$

If V_{p-A} is now replaced, for the sake of argument, by a square well of depth V_0 and radius a, and if $P_\lambda(x)$ is replaced by unity (valid when $R \gg a$ since

then $x \approx 1$), one obtains for v_λ

$$v_\lambda(R,r) \sim (2\lambda+1)^{1/2}(Rr)^{-1} V_0 \tfrac{1}{2}[a^2 - (R-\tfrac{1}{2}r)^2], \quad |R-\tfrac{1}{2}r| \leq a, \tag{22}$$

$$= 0, \quad |R-\tfrac{1}{2}r| > a,$$

which illustrates the properties of $v_\lambda(r,R)$ stated above.

When the value of R is less than or equal to the range a of the optical potentials, then $v_\lambda(R,r)$ will be appreciable for all values of r less than $2(R+a)$, and the R dependence of the transition potential depends intimately on the form of the radial dependence of the optical potentials. As an example of the above considerations concerning $v_\lambda(R,r)$, the case of an exponential nucleon optical potential

$$V_{p-A}(r_p) = V_0 \exp(-Br_p) \tag{23}$$

will now be considered. For this case it can be shown that

$$v_\lambda(R,r) = -\sqrt{2}(2\lambda+1)^{1/2} V_0 (Rr)^{-1/2} \times \frac{\partial}{\partial B} I_{\lambda+1/2}(z) K_{\lambda+1/2}(Z), \tag{24}$$

where Z and z are the larger and smaller, respectively, of the quantities BR and $\frac{1}{2}Br$, and I_ν and K_ν are modified Bessel functions[16] of order $\nu = \lambda + \frac{1}{2}$. When both $\lambda < BR$ and $\lambda < \frac{1}{2}Br$, so that the asymptotic forms of the function I_ν and K_ν can be used, then v_λ becomes approximately independent of λ [apart from the factor $(2\lambda+1)^{1/2}$] and is given by

$$v_\lambda(R,r) \sim -(2\lambda+1)^{1/2}(V_0/Rr) \times \frac{\partial}{\partial B}\{B^{-1}\exp[-B|R-\tfrac{1}{2}r|]\},$$

where terms of the type $\exp[-B(R+\frac{1}{2}r)]$ were neglected. The above result illustrates that when $R \gg \lambda B^{-1}$, $v_\lambda(R,r)$ becomes rather insensitive to λ, and also that $v_\lambda(R,r)$ becomes small when $\frac{1}{2}r$ differs from R by much more than B^{-1}.

An idea of the R dependence of $V^\lambda_{ll'}(k,k',R)$ for large values of R can now be obtained from the above-mentioned properties of $v_\lambda(R,r)$. Since when $R \gg a$, $v_\lambda(R,r)$ is appreciable only for r in the interval $R-a < \frac{1}{2}r < R+a$, it is the value of $u_l(k,r)$ and $u_{l'}(k,r)$ for r lying in this interval that contribute mainly to the integral in Eq. (17) for $V^\lambda_{ll'}$. When both l and l' are small enough so that both u_l and $u_{l'}$ are beyond their turning point in the above-mentioned interval of r, i.e., when $2kR > l$ and $2k'R > l'$, then the product $u_l u_{l'}$ can be approximately represented by terms of the form $\cos[(k-k')r - \delta_-] - \cos[2(k+k')r - \delta_+]$, and then $V^\lambda_{ll'}(k,k',R)$ will become proportional to terms of the type $R^{-2}\cos[2(k \pm k)R + \Delta_\pm]$. The proportionality constants are akin to Fourier transforms of $v_\lambda(R,r)$ for Fourier momenta $k \pm k'$ which in turn are related to Fourier transforms of the nucleon-nucleus optical potentials. This point is made more precise later on. When $k \sim k'$ [or more precisely, when $2(k-k')a \ll \pi$] then the term in $R^{-2}\cos[2(k-k')R + \Delta_-]$ will become nearly independent of k and k', as can be seen by carrying out the integrations for $V^\lambda_{ll'}$ in Eq. (17a) using for $v_\lambda(R,r)$ the approximate form given by Eq. (22) for the square-well example. A similar argument should also hold for (small) distances of R of about the range of the optical potential. In this case the range of r for which $v_\lambda(R,r)$ is nonnegligible is about twice that ($r \sim 2a$), and provided that both $2ak > l$ and $2ak' > l'$, the oscillatory approximation for $u_l u_{l'}$ stated above should hold for a significant part of the range of integration in Eq. (17), and the magnitude of the result should be only a weak function of k and k'. Of course in this case the R dependence of $V^\lambda_{ll'}(R)$ is no longer of the form R^{-2}. Illustrative results of $V^\lambda_{ll'}$ for the exponential nucleon optical potential will be given below.

On the other hand, when either one or both values of l are so large that $2kR \ll l$ or $2k'R \ll l'$ (and R is still large compared to a), then $u_l u_{l'}$ for $r \sim 2R$ will be small compared to unity, and $V^\lambda_{ll'}(k,k',R)$ will also be small and will increase with increasing R until both $u_l(2kR)$ and $u_{l'}(2k'R)$ again become oscillatory functions of R of nearly unit magnitude, in which case the $R^{-2}\cos[2(k \pm k')R]$ behavior will again set in.

If one of the u's corresponds to the bound (deuteron) case, then at large values of r, u_b decreases exponentially like $\exp(-br)$, with $b \sim 0.231$ fm^{-1}, and $V^0_{0l}(b,k,R)$, the bound-to-continuum transition potential, is expected to contain the factor $R^{-2} \times \exp(-2bR)$ for large values of R. The k dependence of the coefficient will be related to the Fourier transform of the product $u_b(r)v_\lambda(R,r)$ with Fourier momentum k. However, the latter is not related very directly to the Fourier transform of the nucleon optical potentials, as will be discussed further on. In addition to the term in $V^0_{0l}(b,k,R)$ of the type $R^{-2}\exp(-2bR)$ discussed above, there will be others due to the small, but in this case nonnegligible, value of $v_\lambda(R,r)$ for small values of r, even when R is large. The presence of such terms is seen for the exponential example which will now be discussed. These terms would be less easy to see for a Gaussian optical potential, since such a potential falls off with distance much faster than the deuteron bound-state radial function.

The properties of $V^\lambda_{ll'}$ discussed above will now be illustrated by taking for V_{p-A} the exponential form given in Eq. (23), and by approximating the

functions $u_l(k,r)$ and $u_b(r)$ by

$$u_l(k,r) = (2/\pi)^{1/2} kr j_l(kr), \tag{25}$$

$$u_b(r) = M[\exp(-br) - \exp(-b'r)]. \tag{26}$$

Here b' is approximately equal to 1.5 fm^{-1}, M is a normalization constant, and j is the spherical Bessel function. Using the exact expression for v_λ given by Eq. (24) and carrying out the integrations explicitly, one obtains in this case, for $\lambda = l = l' = 0$, the following results. For $R|k-k'| \gg 1$ one obtains

$$V^0_{00}(k,k',R) \approx 4V_0^N \frac{B}{\pi R^2}\left\{\frac{\cos[2(k-k')R]}{[B^2+4(k-k')^2]^2} - \frac{\cos[2(k+k')R]}{[B^2+4(k+k')^2]^2}\right\}. \tag{27}$$

For $BR \ll 1$ and $R(k+k') \ll 1$ one obtains

$$V^0_{00}(k,k',R) \approx \frac{(2/\pi)V_0^N Bkk'}{[\frac{1}{4}B^2+(k-k')^2][\frac{1}{4}B^2+(k+k')^2]}. \tag{28a}$$

For $BR \ll 1$, $R|k-k'| \ll 1$, and $R(k+k') \gg 1$ one obtains

$$V^0_{00}(k,k',R) \approx \frac{4}{\pi B} V_0^N\left\{\frac{B^2}{[B^2+4(k-k')^2]} + \tfrac{1}{3}B^2R^2 \ln[B^2R^2+4(k-k')^2R^2] - \left(\frac{B^2R^{-2}}{[B^2+4(k+k')^2]^2}\right)\cos[2(k+k')R]\right\}. \tag{28b}$$

The results in Eqs. (27) and (28b) illustrate the insensitivity of the magnitude of $V^0_{00}(k,k',R)$ to both k and k' when $|k-k'| \ll \frac{1}{2}B$ and $(k+k') \gg \frac{1}{2}B$. In Eq. (27) the R^{-2} dependence is also to be noted. When the average of $V^0_{00}(k,k',R)$ over k' in an interval Δ around k is considered, the first term in Eq. (27) gives

$$\int_0^\Delta V^0_{00}(k,k+x,R)dx \approx \frac{V_0^N B}{8\pi R^3}\frac{\sin(2R\Delta)}{[\frac{1}{4}B^2+\Delta^2]^2}, \tag{29}$$

which shows that the averaging process introduces another factor of R^{-1} for distances larger than $\frac{1}{4}\pi/\Delta$. This property is expected to be valid also for more realistic potentials, provided that the size of Δ is less than the inverse of a characteristic dimension of the potential.

For the bound-to-continuum transition, assuming that $b > \frac{1}{2}B$, one obtains for $R \ll |b \pm \frac{1}{2}B + ik|^{-1}$

$$V^0_{00}(b,k,R) \approx M(2/\pi)^{1/2} V_0^N\left\{\frac{k}{[(b+\frac{1}{2}B)^2+k^2]} - \frac{k}{[(b'+\frac{1}{2}B)^2+k^2]}\right\} \tag{30}$$

and for $R \gg |b \pm \frac{1}{2}B + ik|^{-1}$

$$V^0_{00}(b,k,R) \approx M(2/\pi)^{1/2} V_0^N\left\{\left[\frac{1}{B}e^{-BR}\tan^{-1}\left(\frac{Bk}{b^2+k^2-\frac{1}{4}B^2}\right)\right.\right.$$
$$\left.\left. -\frac{1}{R^2}e^{-2bR}\frac{\partial}{\partial B}\left(\frac{-bk\cos(2kR)+\frac{1}{2}(\frac{1}{4}B^2+k^2-b^2)\sin(2kR)}{(k^2+b^2+\frac{1}{4}B^2)^2-B^2b^2}\right)\right] - [b \to b']\right\} \tag{31}$$

for small and large values of R, respectively. The result in Eq. (31) contains the $R^{-2}\exp(-2bR)$ term and the additional term $\exp(-BR)$, both expected to be present in view of the general discussion made above.

The momentum dependence of the transition potentials is of importance in order to ascertain the errors involved in the truncation of the momentum continuum for $k > k_{\max}$, as is discussed in connection with Eq. (14). The general considerations concerning the momentum dependence of the transition potentials, discussed above, can be made more precise in the case that the $u_l(k,r)$ and $u_b(r)$ are approximated by spherical Bessel functions and exponentials, as in Eqs. (25) and (26), respectively.[17] As shown in the Appendix, the transition potentials can in this case be expressed exactly in terms of integrals involving the Fourier transforms $v_p(K)$ and $v_n(K)$ of the optical potentials

$$v_p(K) = \int V_{p-A}(r_p)e^{-i\vec{K}\cdot\vec{r}_p}d^3r_p \tag{32a}$$

through the combination

$$v_N^\lambda(K) = v_p(K) + (-)^\lambda v_n(-K). \tag{32b}$$

It is also shown in the Appendix that when k and k' become very different from each other, $V^\lambda_{ll'}(k,k',R)$ is expected to decrease roughly like $v_N^\lambda(2k)$, where k is the larger of the two momenta, provided that $\lambda \ll 2kR$. This behavior is already exhibited in the

exponential example, given in Eq. (27), since in this case the expression $8\pi B(B^2+4k^2)^{-2}$ is equal to $v_N^\lambda(2k)$. As a result, it is expected that the coupling between two continua which differ appreciably in k will not be important. On the other hand, it is believed that the coupling between neighboring continua, for small enough values of l, l', and λ will in general be large, no matter how large the momenta k and k', provided that the difference between k and k' remains small compared to the inverse of the range (or some other characteristic length) of the nucleon optical potentials.

The momentum dependence of the bound-to-continuum transition potential will now be discussed. In Appendix B an expression relating $V_{0l}^l(b,k,R)$ to the Fourier transforms $v_N^l(K)$ of the optical potentials is established. However, this relation involves an integral over all values of K, and a relation involving only those $v_N^l(K)$'s for which K lies in a small range around k is not obtained. This situation is illustrated by the exponential example given in Eq. (23) for which the function $V_{00}^0(b,k,R)$ has a part given in the first line of Eq. (30) which varies with k like

$$\tan^{-1}[Bk(b^2+k^2-\tfrac{1}{4}B^2)^{-1}]-\tan^{-1}[Bk(b'^2+k^2-\tfrac{1}{4}B^2)^{-1}].$$

This term, which for values of k larger than both b and b' is expected to fall off like k^{-3}, is not related to the Fourier transform $8\pi B/[(k\pm ib)^2+B^2]^2$ of the optical potential, seen to occur approximately in the second line of Eq. (30), and which falls off faster with k. Of course the exponential example is not meant to suggest what k dependence to expect for the more realistic nucleon optical potential of the Woods-Saxon type, which will be treated numerically in the next section. The intuitive reason why the k dependence of $V_{0l}^l(b,k,R)$ is not very directly related to $v_N^l(k)$ is that the bound-state function $u_b(r)$ entering into Eq. (17b), has a Fourier transform which remains large for values of the Fourier momentum of the order of b' ~ 1.5 fm^{-1}, due to the rapid variation of u_b within the rather short range of the nucleon-nucleon potential V_{np}. In order to illustrate the large size of b', it is useful to consider the corresponding value of the relative neutron-proton kinetic energy ϵ_k ($\epsilon_k=\hbar^2k^2/m$) for $k\sim 1.5$ fm^{-1}, which is approximately 100 MeV. This value, when interpreted as a breakup energy, is indeed quite large. The numerical calculation presented in Sec. III B extends to values of k below 1.2 fm^{-1} and the elastic phase shifts calculated in Sec. IV include momenta only up to 0.6 fm^{-1}.

B. Numerical examples

Numerical calculations of the transition potentials for the nuclei of Ni and Ca will now be discussed. The incident deuteron energy is 21.6 MeV, and the parameters for the nucleon-nucleus potentials at 10.8 MeV, required for the calculation of V_N, Eq. (10), are taken from studies by Buck,[18] Perey,[18,19] and Rosen *et al.*,[20] and are listed in Table I. The functions $u_l(k,r)$ and $u_b(r)$ are calculated numerically from Eqs. (3) and (5) by utilizing the local V_{np} potential given by Eq. (4), for values of r up to $r_{\max}=40$ fm. The spherical harmonic components $v_\lambda(R,r)$ of V_N defined in Eq. (18) are calculated numerically according to

$$v_\lambda(R,r)=\frac{(2\lambda+1)^{1/2}}{rR}\times\int_{x_1}^{x_2}x[V_{p-A}(x)+(-)^\lambda V_{n-A}(x)]P_\lambda(u)dx, \tag{33}$$

where

$$u=(R^2+\tfrac{1}{4}r^2-x^2)/(Rr),$$

$$x_1=|R-\tfrac{1}{2}r|\,,\quad x_2=R+\tfrac{1}{2}r\,.$$

The transition matrix elements defined in Eqs. (17) are calculated by numerical integration over r from 0 to $r_{\max}$. The neglected contributions from the region of integration beyond $r_{\max}$ decrease like $\exp[(R-\frac{1}{2}r_{\max})/a]$ for an exponentially decaying tail of $V_N(x)\sim V_0^N\exp(-x/a)$. The above error estimate is applicable provided that R is smaller than $\frac{1}{2}r_{\max}$ minus the range of the optical potentials. For values of $r_{\max}$ of 40 fm, the error in the continuum-to-continuum transition potentials for Ni is less than 15 and 5% for values of R of 14 and 12 fm, respectively. The errors decrease rapidly for smaller R values, and are smaller for the nucleus of Ca than that of Ni since the optical potential is of shorter range. For the bound-to-continuum transitions the errors are less than for the continuum-to-continuum transitions due to the addi-

TABLE I. Optical potential parameters. The potentials are given by $V(r)=-V_0[1+\exp(r-R)/a]^{-1}-4iW_0\times[1+\exp(r-R')/a']^{-1}\exp(r-R')/a'$.

	V_0 (MeV)	R (fm)	a (fm)	W_0 (MeV)	R' (fm)	a' (fm)
Neutron-nucleus						
Ni [a]	39.58	5.28	0.62	3.75	5.28	0.65
Ca [b]	44.87	4.343	0.66	9.6	4.343	0.47
Proton-nucleus [c]						
Ni	51.6	5.0	0.65	13.16	5.0	0.47
Ca	49.7	4.275	0.65	13.5	4.275	0.47

[a] From Table I of Ref. 18.
[b] From Table V of Ref. 20.
[c] From Ref. 19.

tional damping at large distances arising from the exponential decrease of the bound neutron-proton state. The contribution of the Coulomb interaction to the transition potentials cannot be calculated by the numerical method described above, since the errors introduced by cutting off the integration at r_{max} would be unacceptably large. Instead their evaluation should be based on analytical methods. If included, the Coulomb potential would give relatively larger contributions to $V^{\lambda}_{ll'}$ for odd rather than even values of λ since in the former case the nuclear contributions tend to cancel, while in the latter case they add. An explicit approximate numerical evaluation of $V^{l}_{0l}(b,k,R)$, with inclusion of the Coulomb potential, for Ni with $l=1$ showed that the result is still considerably smaller than the result for either $l=0$ and 2, for distances R comparable to the range of the nuclear optical potentials. This suggests that for incident deuteron energies above the Coulomb barrier, the Coulomb forces should not play a major role in the breakup, and they are left out in the calculations reported on below.

The numerical results obtained for Ni are illustrated in Figs. 1 to 4. In Fig. 1 the real parts of the bound-to-continuum transition matrix elements are shown for various values of the breakup energy ϵ_k. Samples of the continuum-to-continuum transition matrix elements from a state with $\epsilon_k = 5.42$ MeV and $l=0$ or 2 to various states with $l=2$ and several values of $\epsilon_{k'}$ are shown in Fig. 2. The multipole component of V_N whose matrix element gives rise to the results shown in Fig. 2 correspond to $\lambda=2$. Confirming the observations made in Sec. I the transition matrix elements go to zero near the origin, become more oscillatory, and decrease in absolute value as $|k-k'|$ increases. The real parts of the transition matrix elements for the $\lambda=0$ multipole components of V_N are shown in Fig. 3.

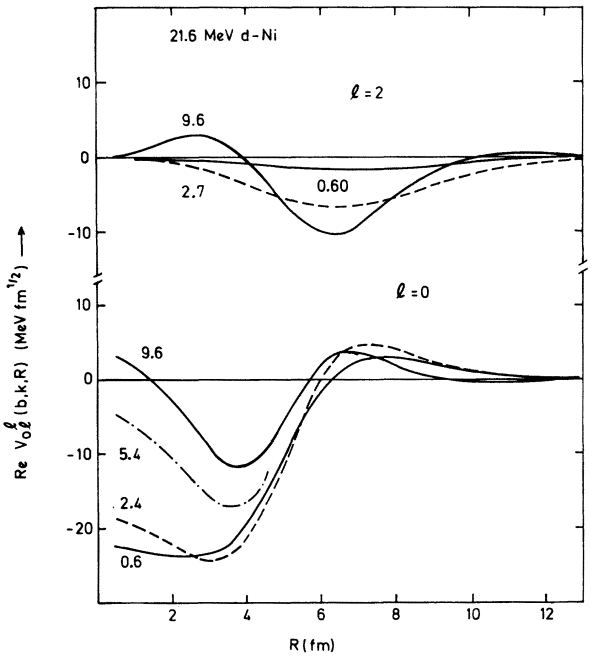

FIG. 1. Real part of the bound-to-continuum breakup transition matrix elements $V^{l}_{0l}(b,k,R)$ for 21.6-MeV deuterons incident on Ni. The matrix elements are defined in Eq. (17b), the values of l are 2 and 0 as shown, and R is the distance of the c.m. of the neutron-proton pair to the center of the nucleus. Each curve illustrates the result for a different value of the relative neutron-proton kinetic energy ϵ_k. The values in MeV of ϵ_k are written next to each curve.

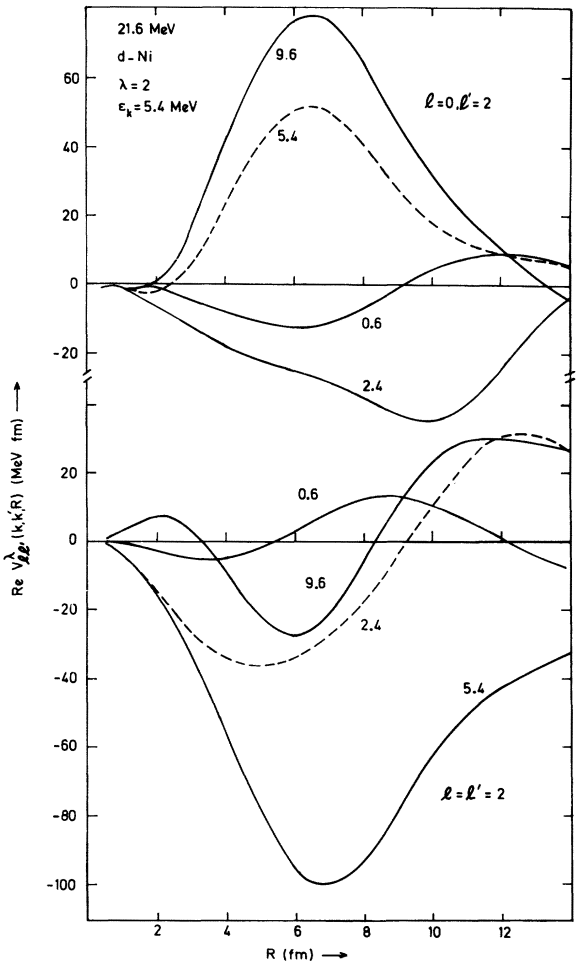

FIG. 2. Real part of continuum-to-continuum transition matrix elements $V^{\lambda}_{ll'}(k,k',R)$ for 21.6-MeV deuterons incident on Ni. The upper set of curves corresponds to $l=0$, $\lambda=l'=2$, the lower set to $l=l'=\lambda=2$. The value of k for all curves is 0.36 fm^{-1}, the corresponding value of ϵ_k is 5.42 MeV. The values of $\epsilon_{k'}$ in MeV which characterize the values of k' are written next to the curves.

These potentials have much larger absolute values (as is seen by the different scale) than the ones shown in Fig. 2.

The momentum dependence of the breakup transition matrix elements is of considerable interest since it determines the value of k_{max} in the k truncation of the wave function Ψ^T, defined in Eq. (14). The k dependence of the bound-to-continuum breakup potential $V^l_{0l}(b,k,R)$ can be deduced from Fig. 4 which shows plots as a function of k of the absolute value of the maxima and minima of $V^l_{0l}(b,k,R)$ which occur as a function of R. As is seen from Fig. 1, the values of R where these extrema occur do not change sensitively with k, and these values of R are indicated in parenthesis next to the various curves. A similar plot for the bound-to-continuum transitions for 21.5-MeV deuterons interacting with Ca is shown in Fig. 5. Comparison with the dash-dot line shows that for k beyond ~0.6 fm^{-1} the $l=0$ transition potentials fall off with k nearly as k^{-2}. This is faster than the k^{-1} dependence which would be expected according to Eqs. (30) and (31) for $b<k<b'$. For the moderately small values of R here involved the exponential potential is evidently not a good approximation to the Woods-Saxon potential. It is clear from Figs. 4 and 5 that the $l=2$ bound-to-continuum transitions are important and even exceed the $l=0$ transition matrix elements for already quite moderate breakup energies, while the $l=4(g)$ transitions are comparatively less important. It also appears that breakup energies ϵ_k up to about 10 MeV do most certainly play a large role in the expansion of Ψ^T, and energies as large as 40 MeV ($k\approx 1$ fm^{-1}) may possibly still be of importance. This point is discussed further in the next section.

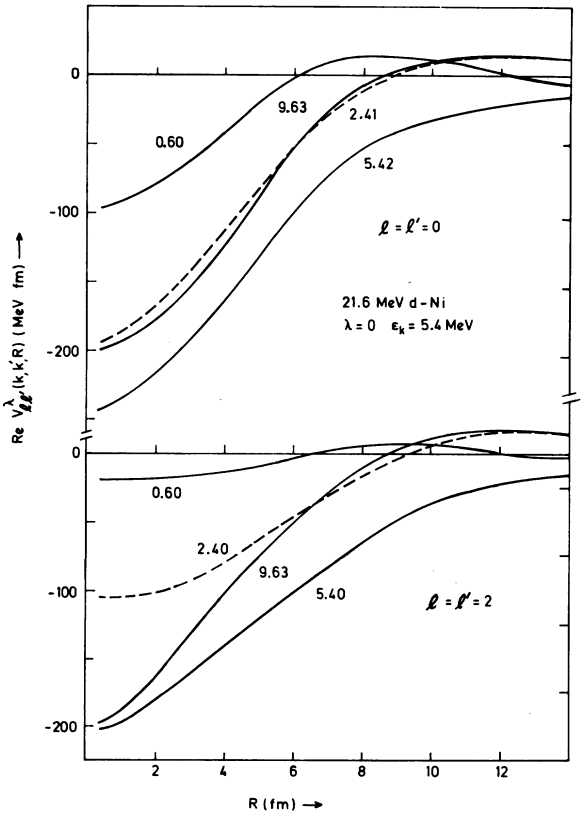

FIG. 3. Real part of the continuum-to-continuum transition matrix elements $V^0_{ll}(k,k',R)$ for 21.6-MeV deuterons incident on Ni. The sets of curves in the upper and lower halves of the figure correspond to values of l of 0 and 2, respectively. The value of k for all curves is 0.36 fm^{-1}, which corresponds to $\epsilon_k = 5.42$ MeV. The values in MeV of $\epsilon_{k'}$ are indicated next to each curve.

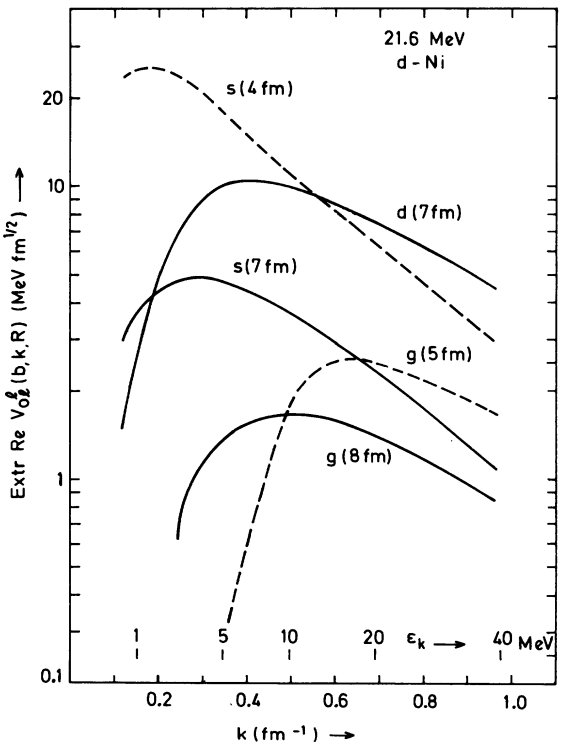

FIG. 4. Momentum dependence of the bound-to-continuum transition matrix elements $V^l_{0l}(b,k,R)$ for 21.6-MeV deuterons incident on Ni. The quantities $V^l_{0l}(b,k,R)$ have maxima and minima when considered as a function of R, as can be seen from Fig. 1. The absolute value of these extrema is plotted versus k in the present figure. The corresponding values of $\epsilon_{k'}$ are illustrated in the second horizontal scale. The letters s, d, and g indicate the values of l, which are 0, 2, and 4, respectively. The numbers in parenthesis next to each letter indicate the approximate value of R where the extremum of $V^l_{0l}(b,k,R)$ occurs.

IV. EFFECT OF BREAKUP ON THE ELASTIC PHASE SHIFTS

The magnitude of the effect on the elastic deuteron wave function due to virtual transitions to breakup states can of course not be assessed alone by the magnitude of the bound-to-continuum breakup transition matrix elements, since Green functions and transitions to other intermediate continuum states are also involved in the solution of the coupled equations [Eqs. (15)]. However, before Eqs. (15) can be solved, this infinite set of equations must be reduced to a finite one by replacing the continuum variable k by a set of discrete variables. In the present study this is accomplished by dividing the range of k between 0 and k_{max} into bins of size Δk and by considering the averages of the wave functions $f_{(lL)J}(k,R)$, the energies ϵ_k, and the transition matrix elements $V^{\lambda}_{ll'}(k,k',R)$ in each bin. In the present study this averaging procedure is done rather crudely, in order to assess the influence of the $l=2$ breakup states on the elastic phase shifts, and in order to gain an idea how large k_{max} should be.

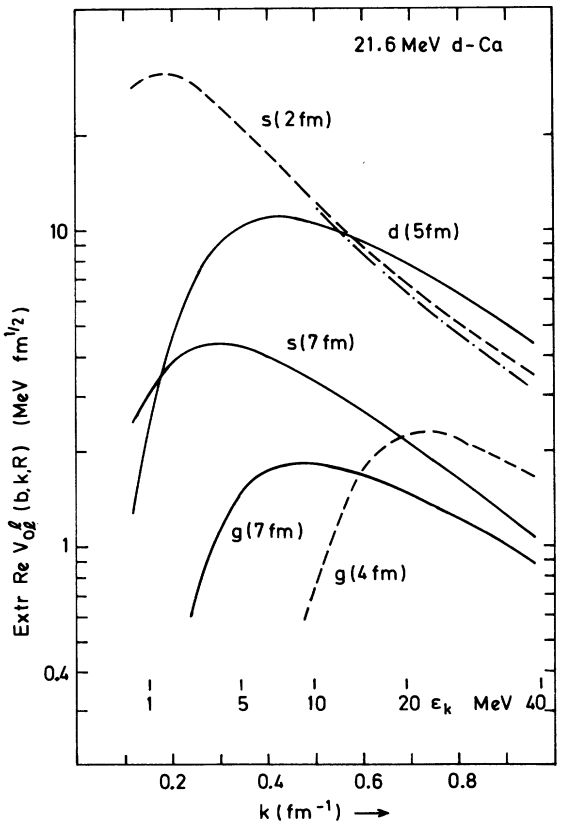

FIG. 5. Same as Fig. 4 for 21.6-MeV deuterons incident on Ca. The dash-dot curve drawn next to the s(2 fm) curve illustrates a k^{-2} dependence.

A. Momentum discretization

Each momentum bin of size Δk (for k contained between 0 and k_{max}) is denoted by $s=1,2,\ldots N$. In each bin a radial wave function $f_{(lL)J}(s,R)$ is defined, which is related to a certain momentum-averaged value of the true (but unknown) function according to

$$f_{(lL)J}(s,R)=(\Delta k)^{1/2}f_{(lL)J}(\bar{k}_s,R)\,. \tag{34}$$

The corresponding coupled equations for the functions $f(s,R)$ are obtained by integrating Eqs. (15) over k' within a given bin, and replacing the integrals of the various quantities by average values within each bin. For example, $\int_{\text{bin }s}\epsilon_{k'}f_{(l'L')J'}(k'R)dk'$ is replaced by $\epsilon_s f_{(l'L')J'}(\bar{k}_s,R)\Delta k$, and ϵ_s is replaced by some constant, even though rigorously ϵ_s should be a function of R which depends on the value of f.

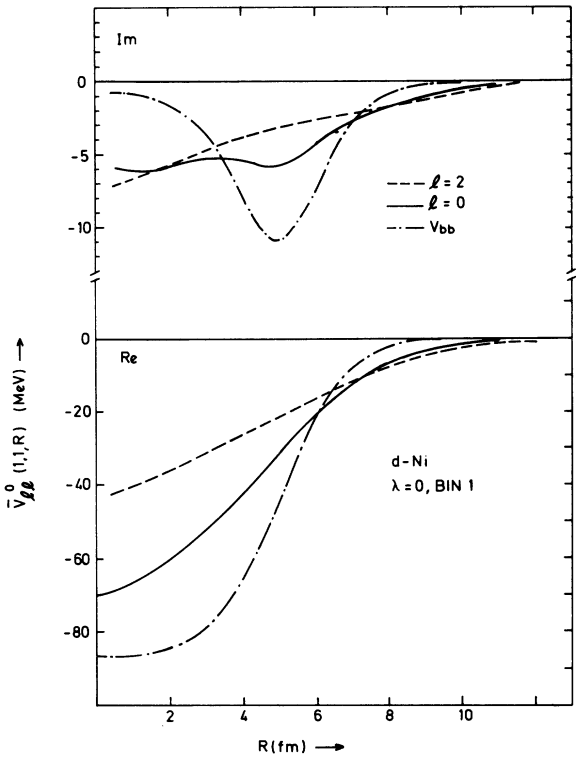

FIG. 6. Momentum-averaged continuum-to-continuum central potentials for 21.6-MeV deuterons incident on Ni. The potentials illustrated are $\bar{V}^{\lambda}_{ll'}(s,s',R)$ for $\lambda=0$ and $l=l'$ having the values 2 and 0 for the dashed and solid curves, respectively. The momentum-averaging bin, characterized by $s=s'=1$, spans the range $0.06\ \text{fm}^{-1}\le k\le 0.54\ \text{fm}^{-1}$. The real and imaginary parts of these potentials are illustrated in the lower and top halves of the figure, respectively. The scales for each half of the figures are not the same. The dash-dotted curves illustrate the Watanabe potential $V_{bb}\equiv V^{0}_{00}(b,b,R)$ defined in Eq. (17b), which of course is not averaged over momentum.

In the numerical calculation described below, a rather large value of 0.48 fm^{-1} is taken for Δk. In a similar fashion, the momentum-averaged transition potentials are calculated by subdividing each bin into n equal intervals of size $\delta k = \Delta k/n$. The n values of k at the center of each interval in bin s are denoted by $k_1^s, k_2^s, \ldots, k_n^s$, and the n^2 values of $V^{\lambda}_{l'l}(k', k, R)$ are calculated at these points. The averaged (or discretized) transition potentials are then defined according to

$$\bar{V}^{\lambda}_{l'l}(s', s, R) = \frac{\Delta k}{n^2} \sum_{i,j=1}^{n} V^{\lambda}_{l'l}(k_i^{s'}, k_j^s, R), \tag{35a}$$

$$\bar{V}^{l}_{0l}(s, b, R) = \frac{(\Delta k)^{1/2}}{n} \sum_{i=1}^{n} V^{l}_{0l}(k_i^s, b, R). \tag{35b}$$

The factor $(\Delta k)^{1/2}$ in the definitions of the radial wave function, Eq. (34), is convenient because the dimension of the resulting functions $f(s,R)$ is the same as that of the (bound-state) wave function $f_{(0L)J}(b,R)$. Similarly the "discretized" transition potentials given in Eqs. (35) have the same dimensions as $V_{bb}(R)$, i.e., energy.

For the discussion which follows, it is convenient to rewrite the "discretized" coupled equations thus obtained in the simplified form

$$(T_R - E_b + V_{bb})\chi_b + \sum_{l,s} \bar{V}^{l}_{bs}\chi^{l}_{s} = 0, \tag{36a}$$

$$(T_R - E_{s'} + \bar{V}^{l'}_{s's'})\chi^{l'}_{s'} + \sum_{\substack{ls \\ s \neq s'}} \bar{V}^{l'l}_{s's}\chi^{l}_{s} + \bar{V}^{l'}_{bs'}\chi_b = 0, \tag{36b}$$

where the χ_s's stand short for the $f_{(lL)J}(s,R)$'s while $\bar{V}^{l'l}_{s's}$ and $\bar{V}^{l}_{s's}$ represent $\bar{V}^{\lambda}_{(l'l)}(s', s, R)$ and $\bar{V}^{0}_{ll}(s', s, R)$, respectively, $E_s = E_b - \epsilon_s$, and the vector addition coefficients C are suppressed. Since the continuum-to-continuum transitions are large for neighboring momenta, the averaged potentials $\bar{V}_{ss'}$ with $s = s'$ are larger than for $s \neq s'$. The former ones (with $s = s'$ and $\lambda = 0$) are thus considered as central potentials and are placed inside the round brackets in Eq. (36b). Taking for n the value 4, the values of k in the four intervals in the first bin are 0.12, 0.24, 0.36, and 0.48 fm^{-1} and the corresponding values of ϵ_k are 0.601, 2.41,

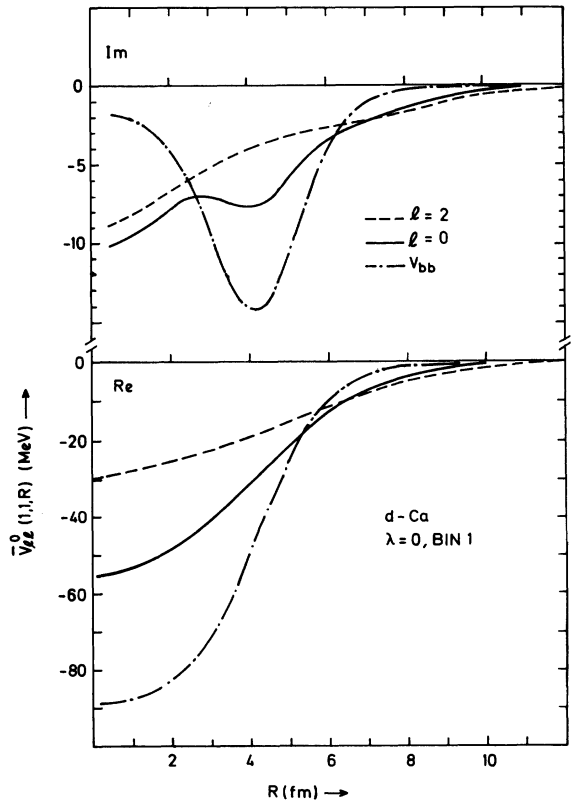

FIG. 7. Same as Fig. 6 for the target of Ca.

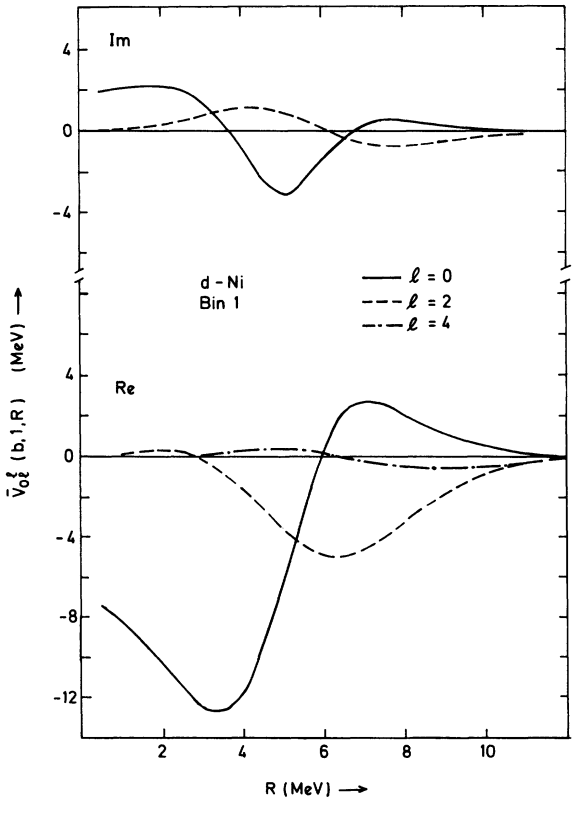

FIG. 8. Momentum-averaged bound-to-continuum breakup potentials for 21.6-MeV deuterons incident on Ni. The potentials illustrated are $\bar{V}^{l}_{0l}(s, b, R)$ defined in Eq. (35b), the value of l being indicated in the figure. The momentum-averaging bin is the one for $s=1$, i.e., $0.06 \leq k \leq 0.54$ fm^{-1}. The real and imaginary parts are shown in the lower and upper halves of the figure, respectively.

5.42, and 9.63 MeV, respectively. In the second bin the corresponding quantities have the values $k = 0.60$, 0.72, 0.84, 0.96 fm^{-1} and 15.05, 21.68, 29.5, and 38.6 MeV, respectively.

An interval length δk of $\frac{1}{4}\Delta k = 0.12$ fm^{-1} was chosen so that the four points in a bin run across a complete wave length of the oscillatory transition matrix elements for a distance R of about 8 fm. It was thus hoped that the averaging procedure of Eq. (35) would thereby achieve a rough cancellation of the oscillatory part of the transition potentials beyond 8 fm. Indeed, the resulting average potentials are reasonably smooth functions of R, as is seen from Figs. 6 to 9.

The real and imaginary parts of the averaged central potentials are displayed in Figs. 6 and 7 for the nuclei of Ca and Ni, respectively. The potentials result by averaging the $\lambda = 0$ continuum-to-continuum transition matrix elements according to Eqs. (35). The averaged bound-to-continuum and continuum-to-continuum transition matrix elements obtained with $\lambda = 2$ for Ni are shown in Figs. 8 and 9, respectively. The corresponding results for Ca (not shown) are quite similar, with the exception that they are shifted by about one fm to smaller values of R. By comparing the magnitudes of the potentials displayed in Figs. 8 and 9, one can observe that the continuum is coupled to itself rather strongly, more strongly than the coupling between the bound to the continuum. The momentum—or bin—dependence of the bound-to-continuum averaged transition potentials is illustrated in Fig. 10. For the higher momentum bin the averaged potentials have oscillations in R of shorter wave length, in agreement with the analytical example discussed above. While the bin 2 $l = 0$ transition potential is already considerably smaller in magnitude than the corresponding bin 1 result, this is not yet the case for the $l = 2$ potentials. However, according to Fig. 4, a considerable reduction in magnitude is to be expected for the next bin for the $l = 2$ case also. The diagonal potentials also show a considerable momentum dependence. For example, for the continuum-to-continuum transition $l = 0$ to $l = 0$ (with $\lambda = 0$) the real part of the averaged transition potential has a depth of about 56 MeV in bin 1, for the nucleus of Ca. For bin 2 the same transition potential has a depth of 75 MeV and a somewhat shorter range, its value becoming smaller than the bin 1 result beyond 5.5 fm. For the $\lambda = 0$, $l = l' = 2$ Ca case the

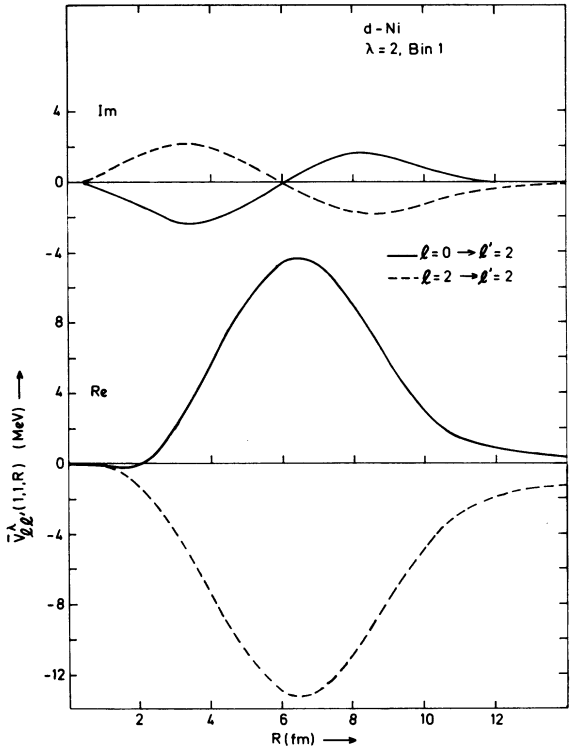

FIG. 9. Momentum-averaged continuum-to-continuum breakup potentials, $\bar{V}^{\lambda}_{ll'}(s, s', R)$. Here $\lambda = 2$, and the transitions from $l = 0$ to $l' = 2$ and $l = 2$ to $l' = 2$ are illustrated by the solid and dashed curves, respectively. The momentum-averaging bin is the one for $s = s' = 1$.

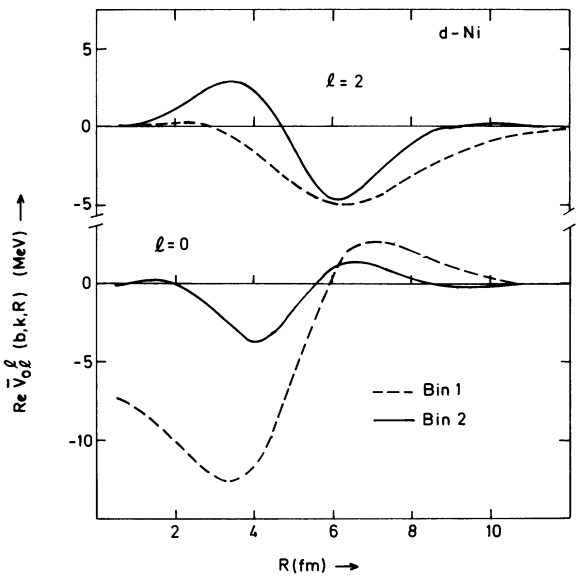

FIG. 10. Bound-to-continuum breakup potentials averaged over two different momentum bins for 21.6-MeV deuterons incident on Ni. Bins $s = 1$ and $s = 2$ are given by the intervals $0.06 \leq k \leq 0.54$ fm^{-1} and $0.54 \leq k \leq 1.12$ fm^{-1}, respectively; the corresponding relative kinetic energies ϵ_k can be read off from Fig. 4. The real parts of $\bar{V}^{l}_{0l}(s, b, R)$ with $s = 1$ and 2 are illustrated by the dashed and solid lines, respectively. The value of l is indicated in the figure.

difference is even more significant. The depths of the averaged potentials are ~29 and 78 MeV for the bin 1 and bin 2 cases, respectively, the two potentials crossing over at about 6 fm.

The k averaging procedure described above is extremely crude. The size of the momentum bins Δk has an effect on the R dependence of the average potentials, in particular that of their long range behavior. The smaller the size of Δk, the larger is the distance R beyond which the long range oscillatory R dependence is changed from a R^{-2} to a R^{-3} falloff, as is illustrated by Eq. (29). Hence the elastic phase shifts obtained from the solution of the k-discretized coupled equations may be quite sensitive to the choice of the bin size Δk. A more careful k averaging could be accomplished for example by means of the use of the WKB approximation for the functions $f_{(lL)J}(k,R)$ at large values of R being investigated by Austern and collaborators,[21] or it can be avoided by replacing the continuum set of functions ϕ_k by discrete sets. The latter method is being used by Tandy and Johnson[22] for the calculation of the effect of breakup on stripping cross sections.

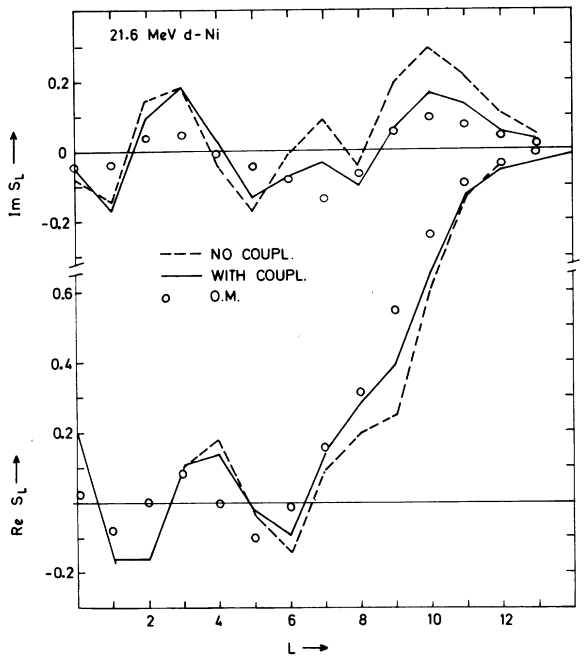

FIG. 11. Elastic deuteron-Ni scattering matrix elements. The curves connect points which represent the values of $S_L = \exp(2iK_L)$ defined in Eq. (37) for discrete values of the deuteron-nucleus orbital angular momenta L. The results without coupling (dashed lines) are obtained with the Watanabe potentials $V_{bb} \equiv V^0_{00}(b, b, R)$ illustrated in Fig. 6. The results with coupling (solid lines) include neutron-proton relative angular momenta l of 0 and 2, together with the bin 1 momentum-averaged transition potentials as is described in the text. The discrete open points represent the optical-model results obtained with the phenomenological parameters of Ref. 23 which approximately fit the experimental cross sections.

B. Elastic phase shifts

The coupled equations, to be solved in this section, have many deficiencies, as is pointed out above. Nevertheless it is hoped that the present results for the effect of breakup states on the elastic phase shifts will serve as a guide for future more reliable calculations. The crudeness of the discretization may not be too serious since errors which occur in the diagonal potentials at large values of R may not give rise to errors in the corresponding Green's functions at small values of R. This is true for example if the JWKB approximation is valid at the large R values. Under this condition one can show that errors in the diagonal breakup potentials in the breakup channels for values of R larger than the range of the bound-to-continuum transition potentials will propagate into the elastic phase shifts only through third and higher order transitions to the breakup states, and hence may be small. An idea of the effect of $k_{\max}$ can be obtained by replacing the function χ^l_s in the second term in Eq. (36a) by an appropriate Green's function integrated over $\bar{V}^l_{sb}\chi_b$ [neglecting coupling to the continuum in Eq. (36b)]. Taking the Green's function outside of the sum one obtains sums of

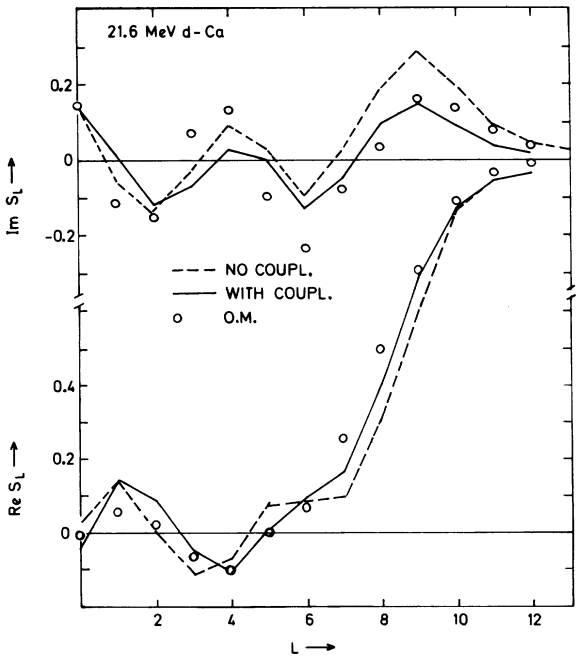

FIG. 12. Same as Fig. 11 for the target of Ca.

the type $\sum_s \overline{V}^l_{bs}\overline{V}^l_{sb}$. If the sum is cut off beyond s_{max}, the error would be of the form $(k_{max})^{-1}$ if one were to assume, in accordance with the previous considerations, that $\overline{V}^l_{bs}$ falls off with k_s as k_s^{-2}. The presence of the Green's function improves the convergence in k_{max}, by introducing another power in k_{max}^{-1}.

The cases of 21.6-MeV deuterons incident on Na and Ca were chosen in order to establish a comparison with the method of JS who also consider these examples.[3,8] The numerical solution of the "discretized" coupled equations is carried out as follows: Coupling of the elastic channel to the $l=0$ and $l=2$ breakup states averaged over the first momentum bin ($0.06 \leq k \leq 0.54$ fm^{-1}) only is included. The average value of ϵ_k in this bin ($0.15 \leq \epsilon_k \leq 12.5$ MeV) is 4.57 MeV, and an approximate value for ϵ_k in this bin of 5 MeV is taken. The coupled equations used are the ones which follow from the discretization of Eqs. (15). The appropriate values of the coefficients $C^{J\lambda}_{L'l';Ll}$, defined in Eq. (16), are used: λ, l, and l' take the values 0 or 2, L and L' are taken as large as required so as to make the elastic phase shifts sufficiently small, which is about 16; the averaged central as well as the transition breakup potentials, shown in Figs. 6–9, are introduced by numerically approximating them by various combinations of Wood-Saxon-like functions and their derivatives. (Thus the expected R^{-2} or R^{-3} long range dependence is suppressed.) Coulomb potentials are added in an *ad hoc* fashion to the central potentials ($\lambda=0$) only, as potentials due to a uniformly distributed charge of radius $R_c=4$ and 5 fm for Ca and Ni, respectively.

The results obtained for the elastic phase shifts are shown in Figs. 11 and 12. They illustrate the real and imaginary parts of the elastic scattering S matrices

$$S_L = \exp(2iK_L), \tag{37}$$

where K_L are the complex nuclear elastic phase shifts for each partial wave of orbital angular momentum L. The discrete points in Figs. 11 and 12 show the results obtained with the phenomenological deuteron optical model. The parameters are taken from the entries of Table II of Perey and Perey,[23] without spin-orbital potential. It can be seen from Figs. 11 and 12 that coupling (solid line) changes the uncoupled values of S_L (dashed lines) towards the optical-model values, particularly for $L \geq 6$. This type of change is also obtained by the method of Johnson and Soper,[3] as will be discussed further below. There is almost no change for $L<6$ in the case of Ni, while for Ca there is considerable change.

The absolute values of the S_L's are the reflection coefficients η_L, which are illustrated in Fig. 13.

It is remarkable that the inclusion of coupling produces a relatively minor enhancement of the absorption coefficients (i.e., a reduction of the η_L's) and that for some partial waves coupling even decreases the amount of deuteron absorption. This is unexpected since normally coupling to additional channels enhances the amount of absorption in the entrance channel. For the full coupled channels this occurs for partial waves 7, 8, and 9 for Ni and 6, 7, 8, and 9 in Ca, while almost for the same partial waves it is also seen to occur for the results obtained with a simulation of the JS method of calculation to be described below. This effect also takes place even if the imaginary parts of the coupling potentials are set to zero and seems to be an inherent feature of the coupling to breakup states. For the "interior" partial waves, i.e., for $L \leq 4$, the effective values of the reflection coefficients both for the coupled and uncoupled calculations hovers in the vicinity of 0.2, i.e., the deuterons propagate through the interior of the nucleus without suffering excessive absorption. The reason is probably that the correlation between the two nucleons is sufficiently reduced when the

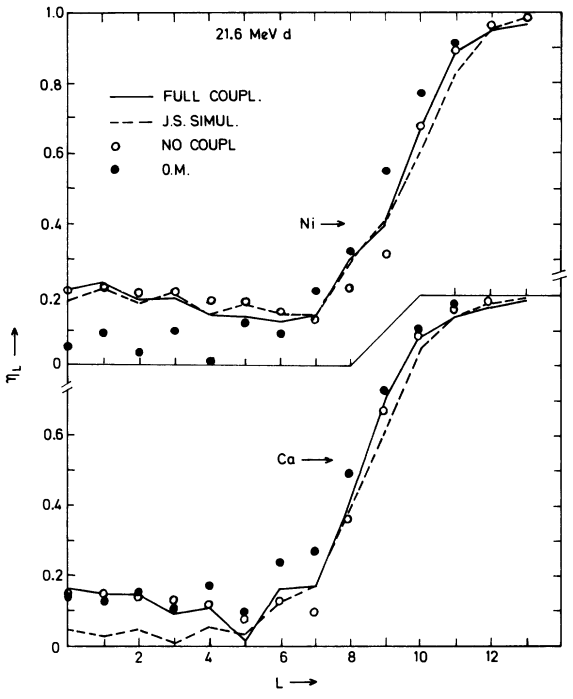

FIG. 13. Reflection coefficients for elastic 21.6-MeV deuteron scattering on Ni and Ca. The full and dashed lines connect results obtained with the full coupled equations and with a simulation of the method of Johnson and Soper, respectively, as is discussed in the text. The open and full circles illustrate, respectively, the results obtained without coupling and the optical-model results.

deuteron is in the broken-up state so that they can propagate throughout the nucleus as if they were independent of each other. Since the antisymmetrization of the incident nucleons with the nucleons in the nucleus will alter the correlation between the two nucleons, it will be quite likely that inclusion of the Pauli exclusion principle[7,24] could have an important effect on the "interior" partial waves. As L increases, the coupled equation values of η_L first decrease to a minimum (near $L=6$ for Ni and 5 for Ca) before increasing again. A similar behavior is found by Rao, Reeves, and Satchler[25] in connection with nonlocal potentials used to represent intermediate inelastic excitations for elastic proton scattering.

The elastic cross sections obtained with the present coupled equations are not in good agreement with experiment. JS reduce the real part of the central potential V_{bb} by 10% in order to achieve a better agreement with experiment. The 10% reduction is supposed to approximately represent the combined effects of the Pauli exclusion principle and of the momentum dependence of the nucleon-nucleus optical potentials.[8,11] A similar reduction of V_{bb} in the present coupled equations improved the agreement of the elastic cross section with experiment for Ni, as can be seen in Fig. 14 from the good agreement with the phenomenological optical-model result. However, for the case of Ca the agreement remained poor, possibly because for this nucleus the effect of the coupling to the stripping channels[26] is too large to be ignored.

C. Comparison with the method of Johnson and Soper

An approximation to the method of JS[3] will now be described. The coupled equations solved by JS are [Eqs. (38) of JS in their notation]

$$(T_R + V_{00} - E_0)\chi_0 + \Delta V \chi_1 = 0\,, \tag{38a}$$

$$[T_R + (\overline{V} - \Delta V) - E_0]\chi_1 + (\overline{V} - V_{00})\chi_0 = 0\,. \tag{38b}$$

Here χ_0 and V_{00} are identical to X_b and V_{bb} in the present paper, and χ_1 is comparable to χ_s^I of Eqs. (36), with $l=0$ and $s=1$. The coupling potentials in Eqs. (38), ΔV and $\overline{V} - V_{00}$, both have a R dependence which is similar in shape to that of the coupling potential $\overline{V}^0_{b1}(R)$ of Eq. (36) [or $\overline{V}^0_{00}(1,b,R)$ of Eqs. (35b)], as can be seen by comparing Fig. 4 of JS with Fig. 8. Further, the magnitude and shape of $[\Delta V(\overline{V} - V_{00})]^{1/2}$ is quite similar to that of $\overline{V}_{00}(1,b,R)$. Hence, if the central potential $\overline{V}^0_{11}(R)$ and the energy E_1 in Eq. (36b) were also set equal, respectively, to $\overline{V} - \Delta V$ and E_0 of Eq. (38b), then χ_1^0 of Eq. (36) would be exactly proportional to χ_1 of Eq. (38), and the solution of Eq. (36) for the elastic wave function in the absence of coupling to the $l=2$ states would be identical to the solution for χ_0 of Eq. (38) of JS. The central potential in the inelastic channel of Eq. (38b), $\overline{V} - \Delta V$, is much closer to V_{00} than is the central potential $\overline{V}^0_{11}[=\overline{V}^0_{00}(1,1,R)]$ of Eq. (36b), as can be seen by comparing the solid and the dash-dot curves in Fig. 6 with the corresponding curves in Fig. 4 of JS. Hence, an approximation to the results of JS can be achieved by replacing E_1 and $\overline{V}^0_{11}$ of Eq. (36b) by E_b and V_{bb}, respectively, and by including in the coupled equations only breakup states with $l=0$. These calculations are denoted by "JS

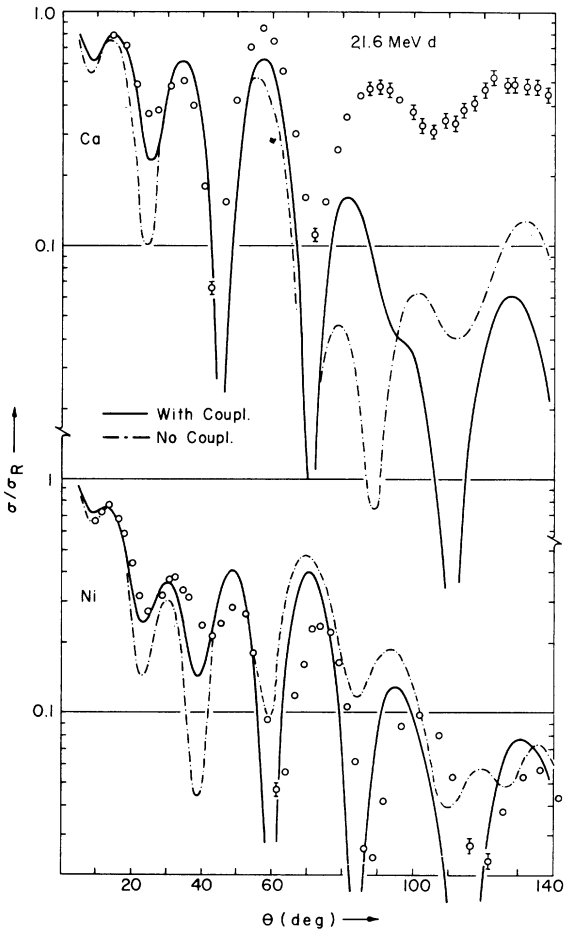

FIG. 14. Elastic deuteron-nucleus cross section divided by the Rutherford cross section, plotted versus scattering angle, for the nuclei of Ca and Ni. The solid lines are obtained with the full set of coupled equations described in the caption to Fig. 11, with the exception that the real part of the deuteron Watanabe potential, V_{bb}, was reduced by 10% in accordance with a prescription given by Johnson and Soper. The dashed lines employ the same potentials in the absence of coupling. The experimental points are taken from Fig. 2 of Ref. 23. The calculations contain no free parameter. As discussed in the text, the effects due to nucleon or deuteron spin are not included in the calculation.

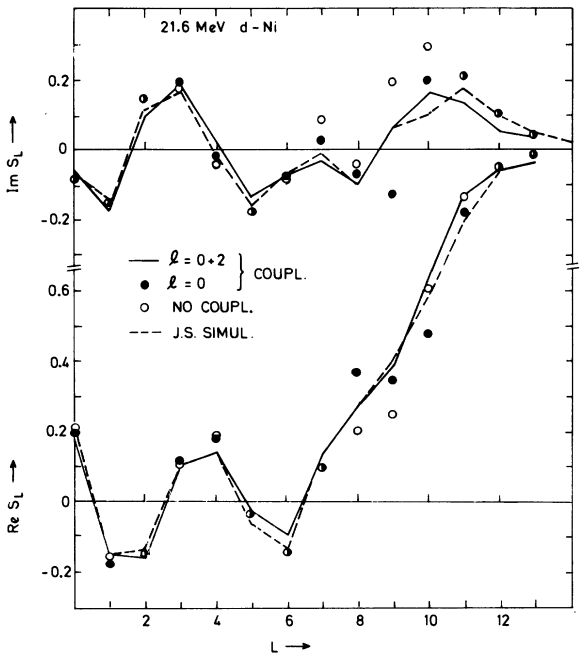

FIG. 15. Elastic scattering matrix elements S_L for 21.6-MeV deuterons incident on Ni. The solid and dashed lines connect values of $\exp(2i K_L)$ obtained, respectively, with the full coupled equations and with a simulation of the Johnson and Soper method described in the text. The full circles illustrate the results of the full coupled equations which, however, include only coupling to the $l=0$ breakup states, while the open circles illustrate the results obtained in the absence of coupling.

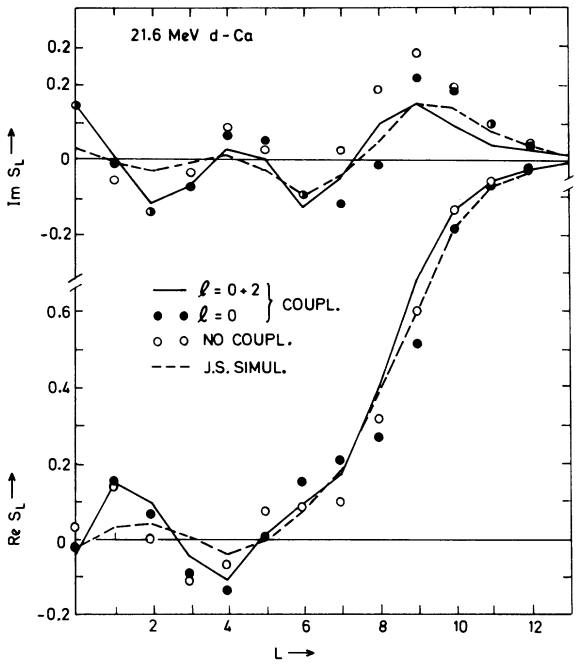

FIG. 16. Same as Fig. 15 for the target of Ca.

simulation" and the results for the elastic scattering elements S_L are shown in Figs. 15 and 16 by the dashed lines. The solid lines indicate the results of the full coupled equations, already shown in Figs. 11 and 12.

Comparison between the full and dashed lines in Figs. 13, 15, and 16 shows a remarkable agreement between the simpler method of calculation of JS and the present results. The agreement is of course not perfect. The differences for the large values of L could be due to the fact that the $l=2$ breakup potentials have a longer range than the $l=0$ ones. The effect of the $l=2$ breakup states is quite large. This effect is illustrated by the distance between the discrete full circles and the points connected by the solid lines in Figs. 15 and 16. Without these $l=2$ contributions the good agreement of the elastic phase shifts with the results of the JS simulation would not have been obtained. This last remark suggests that the effects of the several approximations made by JS seem to largely cancel each other. Thus the approximations of neglecting the breakup energy in the coupled equations seems to be compensated to a large extent by the neglect of coupling to the $l=2$ breakup states. It appears that the cancellations mentioned above can be understood in general terms[27] and this point is being investigated further in collaboration with Johnson.

V. SUMMARY AND CONCLUSIONS

The main conclusion of the present investigation is that a large spectrum of breakup states appears to be involved in the description of deuteron-nucleus interactions. This is seen from Figs. 4 and 5, which illustrate that the matrix elements of the breakup potential $V_N(r_n, r_p)$ (the sum of the proton and neutron-nucleus optical potentials) taken between the bound and continuum neutron-proton relative momentum states are large for a considerable range of the relative n-p linear momentum. Breakup energies up to 10 and most likely 40 MeV could be involved. This suggests that simple energy-independent assumptions for the propagator of the wave function for breakup intermediary states are not reliable. Indeed, for the numerical examples of 21.6-MeV deuterons incident on Ni and Ca it was found that the correction to the elastic phase shifts depends sensitively on whether the average n-p kinetic energy for the n-p centers of mass motion in the breakup state was calculated with a Q value equal to zero ($\bar{\epsilon}_k = -2.225$ MeV) or equal to 7.225 MeV ($\bar{\epsilon}_k = 5$ MeV).

If it is found that contributions from breakup states with breakup energies ϵ_k larger than, say, 50 MeV do not sensitively influence the elastic phase shifts, then there is a possibility that the set of coupled equations discussed in the present study may provide a practical way of including the breakup intermediary states (but not the stripping states). This holds provided of course that improvements such as the inclusion of the Coulomb interaction, a finer discretization interval Δk, and a careful examination of what happens in the transition region in which the breakup channel energies change from positive to negative, do not prove too cumbersome. Questions such as the inclusion of the dependence of V_N on the momenta of the nucleons from the broken-up deuteron,[11,12] the inclusion of stripping channels[27] and of the Pauli exclusion principle[7,8,24] remain to be investigated.

It is remarkable that coupling to the breakup channels has a relatively small effect on the reflection coefficients $|S_L|$. This suggests that perhaps an alternative way of including the breakup process would consist in an adaptation of the Born-Oppenheimer method, in which the neutron-proton eigenstates $\phi_k(\vec{r})$ of H_{np}, given by Eq. (3), would be replaced by $\phi_k(\vec{R},\vec{r})$, solutions of $[H_{np}+V_N(\vec{r},\vec{R})-\epsilon_k(R)]\phi_k(\vec{R},\vec{r})=0$ with $\vec{R}$ playing the role of additional parameters.[28] The resulting deuteron-nucleus potential, $V_{bb}(R)+\epsilon_b(R)-\epsilon_b(\infty)$ would then allow for the "stretching" of the deuteron, and would thus include effects of deuteron polarizability on the elastic potential.[1,29] This line of approach might be relevant also to the study of heavy-ion interactions.

A further conclusion of the present study is that the general results of Johnson and Soper[3] for the elastic scattering phase shifts are qualitatively confirmed by the present study. Notable amongst these is the reduction (compared to the results based on the Watanabe potential V_{bb} in the absence of coupling) of the absorption of the deuterons in the elastic channel for a few surface partial waves. This is an effect which appears to be required in order to improve the agreement with the phenomenological optical model results. Furthermore, the present study confirms that the reflection coefficients for the "interior" partial waves are larger than the optical-model ones and are not strongly affected by the breakup channels. Presumably this means that in the nuclear interior the magnitude of the elastic radial waves is larger than that of the optical-model ones.

It would be interesting to investigate whether the $l=2$ breakup states, found in the present study to be strongly coupled to the elastic channel, will also have an effect on the stripping cross sections. The effect might be similar to that due to the $l=2$ component in the bound deuteron state,[30] which results from the presence of the tensor forces neglected here. However, the present method of expanding the wave function would most likely not be suitable for the calculation of the effect of breakup on stripping reactions, since it does not capitalize on the fact that only small values of relative neutron proton distances are important. Instead, other methods such as the one presently under study by Tandy and Johnson,[22] but augmented so as to include the breakup d state effects, would be desirable.

In summary, more insight is being gained on the participation of the breakup states in the deuteron nucleus interaction, but more work is needed before this effect can be reliably calculated.

ACKNOWLEDGMENTS

The hospitality of the Center for Theoretical Physics at Massachusetts Institute of Technology during the fall of 1972 is gratefully acknowledged, and the many useful conversations with its members, particularly A. K. Kerman, provided a very valuable contribution to this work. Similarly, the hospitality at the University of Surrey and a grant from the Science Research Council which supported the author's sojourn in England during the Winter and Summer of 1973 is much appreciated. This investigation owes a great deal to the untiring comments and criticisms of R. C. Johnson, most gratefully acknowledged here. Also, computing help received during the initial stages of calculation from D. Rule at the University of Connecticut was of considerable help. The initial computations were carried out at the University of Connecticut Computing Center, supported in part by Grant No. GJ-9 of the National Science Foundation. The calculations were continued at the computing centers of the Laboratory of Nuclear Science at Massachusetts Institute of Technology and the Rutherford High Energy Laboratory, England. The author is much indebted for the use of these facilities.

APPENDIX A. CONTINUUM-TO-CONTINUUM TRANSITION POTENTIALS

The neutron-proton continuum wave functions $u_l(k,r)$ are now assumed to be given in terms of spherical Bessel functions, according to Eq. (25). In this case the continuum-to-continuum transition potentials $V^{\lambda}_{ll'}(kk'R)$ can be expressed exactly as integrals over the Fourier transforms of the nucleon-nucleus optical potentials $v_p(K)$ and $v_n(K)$

given by Eqs. (32)

$$C_{ll'\lambda}V^{\lambda}_{ll'}(k,k',R) = (2\lambda+1)^{3/2}kk'(2\pi)^{-3}i^{\lambda-l-l'} \times \sum_{m,m'}\begin{pmatrix} l & l' & \lambda \\ m & m' & M \end{pmatrix}\int v^{\lambda}_N(K)j_\lambda(KR)Y^*_{\lambda M}(\hat{K}) \times Y^*_{lm}(k)Y^*_{l'm'}(\hat{k}')d\Omega_k d\Omega_{k'}. \tag{A1}$$

Here

$$\tfrac{1}{2}\vec{K} = \vec{k} + \vec{k}', \tag{A2}$$

$$C_{abc} = [(2a+1)(2b+1)(2c+1)/4\pi]^{1/2}\begin{pmatrix} a & b & c \\ 0 & 0 & 0 \end{pmatrix}, \tag{A3}$$

the j_λ's are spherical Bessel functions, and the quantities $\begin{pmatrix} a & b & c \\ 0 & 0 & 0 \end{pmatrix}$ are Wigner coefficients.[15]

The above equation is derived by considering the integral

$$\int e^{i(\vec{k}+\vec{k}')\cdot\vec{r}}V_N(\vec{R},\vec{r})Y^*_{lm}(\hat{k})Y^*_{l'm'}(\hat{k}') \times Y^*_{\lambda M}(\hat{R})d\Omega_{k'}d\Omega_k d\Omega_R d^3r$$

and evaluating it by two different methods. The first consists in substituting for V_N the expansion in terms of the v_λ's given by Eq. (18), expanding the exponentials in terms of spherical Bessel functions and spherical harmonics, and carrying out the integrals over the argument of the products of two or three spherical harmonics, thus obtaining an expression containing the $V^{\lambda}_{ll'}(k,k',R)$. The other method consists in replacing $V_N(\vec{R},\vec{r})$ by the sum of the nucleon-nucleus optical potentials, Eq. (10), expressing each optical potential in terms of Fourier integrals and then carrying out the integrations over d^3r, thereby obtaining Dirac δ functions in $\frac{1}{2}\vec{K}\pm(\vec{k}+\vec{k}')$, and achieving the result on the right-hand side of Eq. (A1).

In the integral on the right-hand side of Eq. (A1) the magnitude of K ranges from $2|(k-k')|$ to $2(k+k')$. This follows in view of Eq. (A2), if one thinks of first holding the direction of one of the momenta (for example $\vec{k}$) fixed and integrates over the other ($\vec{k}'$). The above remark suggests how to obtain an approximation to Eq. (A1) when one of the momenta, k' for example, is very small compared to the other. Then for a fixed direction $\hat{k}$, the direction and magnitude of K changes very little as $\vec{k}'$ ranges over all directions, and the quantities $v^{\lambda}_N(K)Y^*_{\lambda M}(\hat{K})$ can be considered independent of $\hat{k}'$ during the integration over $d\Omega_{k'}$, provided that $v^{\lambda}_N(K)$ varies sufficiently little as K changes between its upper and lower limits. However, when $2kR \gg \lambda$, $j_\lambda(KR)$ varies sinusoidally and very rapidly with K, and it cannot be taken outside of the integral. Using the approximation $KR = 2kR + 2k'R(\hat{k}\cdot\hat{k}')$ in the argument of $j_\lambda(KR)$, one obtains for even l' the result

$$\int j_\lambda(KR)Y^*_{l'm'}(\hat{k}')d\Omega_{k'} \approx 4\pi i^{l}j_\lambda(2kR)j_{l'}(2k'R), \tag{A4}$$

valid for l' even and $2kR \gg \lambda$. For l' odd a similar expression involving $\cos(2kR - \frac{1}{2}\lambda\pi)$ instead of $\sin(2kR - \frac{1}{2}\lambda\pi)$ is obtained. Inserting the above approximation into Eq. (A1), one obtains the result

$$V^{\lambda}_{ll'}(k,k',R) \approx 4\pi^{-2}kk'(2\lambda+1)^{1/2}i^{\lambda-l} \times v^{\lambda}_N(2k)j_\lambda(2kR)j_{l'}(2k'R), \tag{A5}$$

which could be considered as the leading term in a Taylor series expansion of $V^{\lambda}_{ll'}(k,k',R)$ about $V^{\lambda}_{ll'}(k,k,R)$. When not only $2kR \gg \lambda$ but also $2k'R \gg l'$, then the result becomes proportional to $v^{\lambda}_N(2k)R^{-2}\sin(2kR - \frac{1}{2}\lambda\pi)\sin(2k'R - \frac{1}{2}\lambda\pi)$ which indicates that the k dependence of the magnitude of $V^{\lambda}_{ll'}$ is then mainly given by $v^{\lambda}_N(2k)$. This is a result made use of in Sec. III A.

APPENDIX B. BOUND-TO-CONTINUUM TRANSITION POTENTIALS

In the considerations below, the functions $u_l(k,r)$ and $u_b(r)$ are given by Eqs. (25) and (26), respectively. By considerations similar to those which led to Eq. (A1), one obtains in this case

$$V^{l}_{0l}(b,k,R) = k(2/\pi)^{1/2}\int_0^\infty j_l(KR)v^{l}_N(K)H_l(k,\tfrac{1}{2}K)K^2dK, \tag{B1}$$

where $v^{l}_N(K)$ is defined in Eq. (32b). The function $H_l(k,\frac{1}{2}K)$ arises from the expansion of the Fourier component $\phi_b(\kappa)$ of the bound-state wave function $r^{-1}u_b(r)$,

$$r^{-1}u_b(r) = \int \phi_b(\kappa)e^{i\vec{\kappa}\cdot\vec{r}}d^3r, \tag{B2}$$

in spherical harmonics of the directions of $\vec{k}$ and $\vec{K}$ ($\vec{\kappa} = \vec{k} + \frac{1}{2}\vec{K}$)

$$\phi_b(|\vec{k}+\tfrac{1}{2}\vec{K}|) = \sum_{\lambda,\mu}4\pi(2\lambda+1)^{-1/2}(-)^{\lambda}H_\lambda(k,\tfrac{1}{2}K) \times Y_{\lambda\mu}(\hat{k})Y^*_{\lambda\mu}(\hat{K}). \tag{B3}$$

Using now for $u_b(r)$ the expression of Eq. (26), one obtains for H_λ the result

$$H_\lambda(k,\tfrac{1}{2}K) = (2\pi)^{-3}4\pi M[h_\lambda(b,k,\tfrac{1}{2}K) - h_\lambda(b',k,\tfrac{1}{2}K)] \tag{B4}$$

where $h_\lambda(b, k, \frac{1}{2}K)$ is defined in the expansion

$$[b^2 + (\vec{k} - \tfrac{1}{2}\vec{K})^2]^{-1} = \sum_\lambda (2\lambda+1)^{1/2} h_\lambda(b, k, \tfrac{1}{2}K) P_\lambda(\hat{k}\cdot\hat{K}). \tag{B5}$$

Explicit evaluation of h_λ shows that[17]

$$h_\lambda(b, k, \tfrac{1}{2}K) = (2\lambda+1)^{1/2}(kK)^{-1} Q_\lambda(\beta), \tag{B6}$$

where

$$\beta = (k^2 + \tfrac{1}{4}K^2 + b^2)/(kK) \tag{B7}$$

and where Q_λ is the Legendre function of the second kind.[16]

In contrast to the result (A1), the integral expression given by Eq. (B1) involves values of the Fourier transform of the optical potentials for the whole range from 0 to ∞ of Fourier momenta. Further, the integrand contains branch points in the complex K plane, due to the singularities of Q_l. As long as K stays on the real axis, Q_l never becomes singular since the argument of Q_l always stays larger than unity, its smallest value being equal to $(1 + b^2k^{-2})^{1/2}$. This value of the argument is attained for $\frac{1}{2}K = (k^2 + b^2)^{1/2}$.

The integral representation given by Eq. (B1) can be of practical value when the singularities of the Fourier transforms $v_N^l(K)$ in the complex K plane are in the form of poles, as is the case for the exponential example given by Eq. (23), or for a Coulomb potential which arises from a charge distribution whose Fourier transform has no singularities other than poles. In these cases the integral in Eq. (B1) can be carried out by contour integration provided that a cut is made between the branch points of $Q_l(\beta)$, and the integral around the latter is evaluated numerically. For a point Coulomb case the contribution from the residues is proportional to

$$MZe^2 l!\,(2l+1)^{-1/2}\{[kR^{-1}/(b^2+k^2)]^{l+1} - [b \to b']\}, \tag{B8}$$

where Z is the charge of the (point) nucleus, while rough estimates[17] of the integral around the cut yield a function which oscillates like $\sin(2kR)$ and which appears to decrease exponentially with R. For the exponential case, Eq. (23), the contribution from the residues is proportional to

$$e^{-BR}\{[\tfrac{1}{2}Bk)/(b^2 - \tfrac{1}{4}B^2 + k^2)]^{l+1} - [b \to b']\}.$$

It is tempting to identify this result with the first term of Eq. (30), while the contribution from the cut appears to be related to the second term in Eq. (30).

---

*On leave of absence from The University of Connecticut, Storrs, Connecticut 06268.

† This work is supported in part though funds provided by the U. S. Atomic Energy Commission under Contract AT(11-1)-3069, CTP No. 378.

[1]J. Testoni and L. C. Gomes, Nucl. Phys. 89, 288 (1966).
[2]K. Ueta and K. Hara, Z. Phys. 248, 311 (1971).
[3]R. C. Johnson and P. J. R. Soper, Phys. Rev. C 1, 976 (1970).
[4]G. Bencze and I. Szentpetery, Phys. Lett. 30B, 446 (1969).
[5]G. R. Satchler, Phys. Rev. C 4, 1485 (1971); J. D. Harvey and R. C. Johnson, *ibid.* 3, 636 (1971); G. M. McAllen, W. T. Pinkston, and G. R. Satchler, Particles and Nuclei 1, 412 (1971); B. M. Preedom, Phys. Rev. C 5, 587 (1972).
[6]A preliminary account of the results is given in *Proceedings of the International Conference on Nuclear Physics, Munich, 1973*, edited by J. de Boer and H. J. Mang (North-Holland, Amsterdam/American Elsevier, New York, 1973), Vol. 1, p. 401.
[7]G. Baumgartner, Z. Phys. 204, 17 (1967); J. R. Rook, to be published.
[8]P. J. R. Soper, Ph.D. thesis, University of Surrey, 1968 (unpublished).
[9]I. Reichenstein and Y. C. Tang, Nucl. Phys. A139, 144 (1969).
[10]For example, B. J. Malenka, U. E. Druse, and N. F. Ramsey, Phys. Rev. 91, 1165 (1935).
[11]P. D. Kunz, Phys. Lett. 35B, 16 (1971); R. C. Johnson and P. J. R. Soper, Nucl. Phys. A182, 619 (1972).
[12]N. Austern and K. C. Richards, Ann. Phys. (N. Y.) 49, 309 (1968); M. Bauer and C. Bloch, Phys. Lett. 33B, 155 (1970); F. J. Bloore, Nucl. Phys. 68, 298 (1965).
[13]R. G. Newton, Ann. Phys. (N. Y.) 74, 324 (1972); W. Glöeckle, Nucl. Phys. A141, 620 (1970).
[14]K. Takeuchi, Nucl.Phys. A208 (1973), pp. 1, 21, and46.
[15]D. M. Brink and G. R. Satchler, *Angular Momentum* (Clarendon, Oxford, 1962).
[16]M. Abramowitz and I. A. Stegun, *Handbook of Mathematical Functions* (Dover, New York, 1964).
[17]G. H. Rawitscher, unpublished.
[18]F. G. Perey and B. Buck, Nucl. Phys. 32, 353 (1962).
[19]F. G. Perey, Phys. Rev. 131, 745 (1963).
[20]L. Rosen, J. G. Beery, A. S. Goldhaber, and E. H. Auerbach, Ann. Phys. (N. Y.) 34, 96 (1965).
[21]N. Austern, private communication.
[22]P. C. Tandy and R. C. Johnson, in *Proceedings of the International Conference on Nuclear Physics, Munich, 1973* (see Ref. 6), Vol. 1, p. 422.
[23]C. M. Perey and F. G. Perey, Phys. Rev. 152, 923 (1966).
[24]B. L. Gambhir and J. J. Griffin, Phys. Rev. C 7, 590 (1973).
[25]C. L. Rao, M. Reeves, III, and G. R. Satchler, Nucl. Phys. A207, 182 (1973).
[26]G. H. Rawitscher, Phys. Rev. 163, 1223 (1967); G. H. Rawitscher and S. N. Mukherjee, Ann. Phys. (N. Y.) 68, 57 (1971); T. Ohmura, B. Imanishi, M. Ichimura, and M. Kawai, Progr. Theor. Phys. 41, 391 (1969); 44, 1242 (1970); L. Döhnert, Ann. Phys. (N. Y.) 62, 422 (1971).
[27]R. C. Johnson, private communication.

[28]J. R. Oppenheimer and M. Phillips, Phys. Rev. 48, 500 (1935); C. F. Clement, *ibid.* 128, 2724, 2728 (1962); F. P. Gibson and A. K. Kerman, *ibid.* 145, 758 (1966).

[29]C. F. Clement, Phys. Rev. 128, 2728 (1962); G. Bencze and E. Pietarinen, Phys. Lett. 19, 586 (1965); J. K. Dickens and F. G. Perey, Phys. Rev. 138B, 1083 (1965).

[30]R. C. Johnson and F. D. Santos, Particles and Nuclei 2, 285 (1971); E. Delic and B. A. Robson, Nucl. Phys. A156, 95 (1970); N. Rohrig and W. Haeberli, *ibid.* 206, 225 (1973).